TUBERCULOSIS

Copyright © 2023 The Authors, some rights reserved; exclusive licensee American Association for the Advancement of Science. No claim to original U.S. Government Works

Tobacco smoke exposure recruits inflammatory airspace monocytes that establish permissive lung niches for *Mycobacterium tuberculosis*

Björn Corleis[1,2]†*, Constantine N. Tzouanas[1,3,4]†, Marc H. Wadsworth II[1,3,4], Josalyn L. Cho[5], Alice H. Linder[1]‡, Abigail E. Schiff[6], Björn Zessin[2], Fabian Stei[2], Anca Dorhoi[2], Amy K. Dickey[1,7,8], Benjamin D. Medoff[7]§, Alex K. Shalek[1,3,4,5,9]§, Douglas S. Kwon[1,9,10]§*

Tobacco smoking doubles the risk of active tuberculosis (TB) and accounts for up to 20% of all active TB cases globally. How smoking promotes lung microenvironments permissive to *Mycobacterium tuberculosis* (*Mtb*) growth remains incompletely understood. We investigated primary bronchoalveolar lavage cells from current and never smokers by performing single-cell RNA sequencing (scRNA-seq), flow cytometry, and functional assays. We observed the enrichment of immature inflammatory monocytes in the lungs of smokers compared with nonsmokers. These monocytes exhibited phenotypes consistent with recent recruitment from blood, ongoing differentiation, increased activation, and states similar to those with chronic obstructive pulmonary disease. Using integrative scRNA-seq and flow cytometry, we identified CD93 as a marker for a subset of these newly recruited smoking-associated lung monocytes and further provided evidence that the recruitment of monocytes into the lung was mediated by CCR2-binding chemokines, including CCL11. We also show that these cells exhibit elevated inflammatory responses upon exposure to *Mtb* and accelerated intracellular growth of *Mtb* compared with mature macrophages. This elevated *Mtb* growth could be inhibited by anti-inflammatory small molecules, providing a connection between smoking-induced pro-inflammatory states and permissiveness to *Mtb* growth. Our findings suggest a model in which smoking leads to the recruitment of immature inflammatory monocytes from the periphery to the lung, which results in the accumulation of these *Mtb*-permissive cells in the airway. This work defines how smoking may lead to increased susceptibility to *Mtb* and identifies host-directed therapies to reduce the burden of TB among those who smoke.

INTRODUCTION

Tuberculosis (TB) has infected more than 20% of the global population, and active TB kills 1 to 2 million people every year (*1*). Current treatment regimens are poorly effective and require the administration of multiple antibiotics for months, highlighting the need for a greater mechanistic understanding of disease to inform additional preventative and therapeutic strategies (*2*). The majority of people infected with the causative agent of TB, *Mycobacterium tuberculosis* (*Mtb*), develop subclinical latent TB infection (LTBI), with only 5 to 10% of individuals with LTBI eventually developing clinical disease (*3*). Although several risk factors are linked to active TB and TB mortality, one of the strongest is smoking (*1*). Globally, 1.3 billion people smoke tobacco, which results in an estimated 10 to 20% of all annual active TB cases being attributed to smoking (*4*, *5*). Despite the tremendous contribution of smoking to the worldwide burden of TB, very little is understood about the specific mechanisms by which smoking promotes active TB.

Upon entry, *Mtb* is believed to primarily proliferate within mature alveolar macrophages (AMs). However, the phenotype and metabolic profiles of AMs from tobacco smokers are substantially altered and associated with diminished phagocytosis and antimycobacterial defense mechanisms (*4*, *6*, *7*, *8*, *9*, *10*, *11*). Furthermore, tobacco smoking has been reported to change the cellular composition of other immune lineages in the alveolar space. For instance, we recently reported a relative decrease in the lymphocyte population and an increase in the total number of macrophages in the airspace compartment with smoking (*9*, *12*). However, a comprehensive understanding of which cell types and states are altered with smoking and how these potentially affect the risk of active TB is lacking. A more detailed understanding of how smoking perturbs the composition and state of the lung microenvironment would provide insights into the mechanisms underlying smoking-associated increased risk for active TB and disease progression, as well as potential avenues for the development of host-directed therapies to prevent and treat active TB.

In this study, we demonstrate that tobacco smoking leads to the recruitment of immature inflammatory monocytes to the lung. These recruited monocytes exhibit phenotypic and transcriptional hallmarks of elevated inflammatory responses and the potential to

[1]Ragon Institute of MGH, MIT, and Harvard, Cambridge, MA 02139, USA. [2]Institute of Immunology, Friedrich-Loeffler-Institute, Greifswald-Insel Riems, 17493, Germany. [3]Institute for Medical Engineering & Science (IMES), Department of Chemistry, and Koch Institute for Integrative Cancer Research, MIT, Cambridge, MA 02139, USA. [4]Broad Institute of MIT and Harvard, Cambridge, MA 02139, USA. [5]Roy J. and Lucille A. Carver College of Medicine, Department of Internal Medicine, Division of Pulmonary, Critical Care and Occupational Medicine, University of Iowa, Iowa City, IA 52242, USA. [6]Department of Medicine, Brigham and Women's Hospital, Boston, MA 02115, USA. [7]Division of Pulmonary and Critical Care Medicine, Massachusetts General Hospital, Boston, MA 02114, USA. [8]Department of Medicine, Harvard Medical School, Boston, MA 02115, USA. [9]Department of Immunology, Harvard Medical School, Boston, MA 02115, USA. [10]Division of Infectious Diseases, Massachusetts General Hospital, Boston, MA 02114, USA.
*Corresponding author. Email: bjoern.corleis@fli.de (B.C.); dkwon@mgh.harvard.edu (D.S.K.)
†These authors contributed equally to this work.
‡Present address: Vagelos College of Physicians and Surgeons, Columbia University, New York, NY, USA.
§These authors contributed equally to this work.

Downloaded from https://www.science.org at Massachusetts Institute of Technology on December 07, 2023

differentiate into monocyte-derived macrophages (MDMs). We identify CD93 as a marker for a subset of these newly recruited airspace monocytes and further provide ex vivo evidence that recruitment of these cells into the lung is partially mediated by CCL11 binding to CCR2. We demonstrate that blood and lung monocytes from smokers exhibit elevated inflammatory responses after exposure to *Mtb* and that immature monocytes support increased rates of *Mtb* growth relative to mature macrophages. Furthermore, we show that treatment of these monocytes with anti-inflammatory drugs can inhibit the observed elevated intracellular *Mtb* growth. These findings provide a biological understanding of a mechanism by which smoking increases *Mtb* growth and reveal potential strategies to mitigate the TB burden among tobacco smokers.

RESULTS

Tobacco smoking leads to an increase of monocytes in the airspaces

To explore the effects of smoking on airspace cells in the lung, we characterized bronchoalveolar lavage (BAL) samples from smokers and nonsmokers (table S1) using single-cell RNA sequencing (scRNA-seq), flow cytometry (table S2), and ex vivo functional assays (Fig. 1A). We found that the total cellularity of BAL fluid was significantly ($P = 0.001$) increased in smokers compared with nonsmokers (fig. S1A). We used flow cytometry to identify airspace monocytes, which were distinct from AMs in their size, granularity, and surface expression of CD14 (fig. S1, B and C). There was a sevenfold increase in the number of small [side scatter (SSC)/forward scatter (FSC)^{low}] CD14^{+} airspace monocytes ($P = 0.005$) in smokers versus nonsmokers but no change in AMs (SSC/FSC^{high}CD45^{+} CD14^{low}CD16^{+}), granulocytes (PMN), or T cells (Fig. 1B and fig. S1, B and C). Thus, our data indicate that the increase in total airspace cells was primarily driven by an increase in small CD14^{+} airspace monocytes.

To further characterize the cells across the lung and blood compartments, we performed picowell-based scRNA-seq on BAL and peripheral blood mononuclear cells (PBMCs) from smokers ($n = 5$) and never smokers ($n = 4$). After performing initial quality controls, we retained 20,799 BAL cells and 36,405 PBMCs for further analysis (fig. S2). Dimensionality reduction, unsupervised clustering, and manual annotation identified 16 populations among the BAL samples, with myeloid cells as the predominant cell type (Fig. 1, C and D, and fig. S2, A to C) (*13*, *14*). We chose to prioritize airspace monocytes for further investigation, because they were significantly enriched in the lungs of smokers as measured through both flow cytometry ($P = 0.005$; Fig. 1B) and scRNA-seq ($P = 0.0049$, Dirichlet regression analysis, which accounts for compositional shifts in one cell type necessarily affecting relative proportions of other cell types; fig. S2, D and E). Expression profiles from the airspace monocytes best aligned with monocytes in a previously published blood immune atlas (fig. S3A) (*15*) and exhibited expression of myeloid-associated markers intermediate between that of blood-derived monocytes and AMs (Fig. 1E). We further corroborated our findings by leveraging the Human Lung Cell Atlas (HLCA), a meta-analysis of nine scRNA-seq studies whose "healthy control" dataset contains 96 healthy (smoker, former-smoker, and never-smoker) participants with >400,000 expert-annotated cells from human airway and lung parenchyma (*16*). In this dataset, classical monocytes, nonclassical monocytes, and interstitial macrophages were the top three cell types, with the strongest enrichment with smoking in both univariate analyses and multivariate Dirichlet regression analysis; their abundances were not associated with age or biological sex in the HLCA (fig. S3, B to F).

To understand the differentiation potential of airspace monocytes, we conducted RNA velocity analyses, which leverage unspliced-to-spliced mRNA ratios to infer cells' dynamic trajectories from scRNA-seq readouts (*17*, *18*). In this approach, a gene with a high unspliced-to-spliced mRNA ratio would indicate recent transcriptional activation and potential information about a cell's future state. RNA velocity analyses indicated that airspace monocytes are an immature cell type with the capacity to differentiate into more mature macrophage populations, with trajectories originating in the airspace monocyte cluster and moving toward more mature macrophage cell clusters (macrophage 5 and macrophage 6; Fig. 1F). Consistent with the notion that these airspace monocytes are an infiltrating, immature population associated with smoking that then matures into specific macrophage lineages, macrophage 5 and macrophage 6 populations (the macrophage clusters predicted to be descendants of airspace monocytes) were also enriched in samples from smokers compared with never smokers (airspace monocytes – $P = 4.9 \times 10^{-3}$, macrophage 5 – $P = 6.1 \times 10^{-5}$; macrophage 6 – $P = 7.3 \times 10^{-6}$; Dirichlet regression analysis; fig. S2, D and E), highlighting specific macrophage subsets that accumulate with smoking-mediated monocyte recruitment.

As compared with blood monocytes, both airspace monocytes and macrophages exhibited elevated expression of gene sets related to macrophage function (e.g., phagocytosis and antigen processing/presentation) (Fig. 1G and fig. S4A), supporting the interpretation that airspace monocytes are a differentiating cell population. As external support from a separate human disease cohort, we compared the airspace monocyte population in this study against work from Baßler *et al.* (*19*), who identified a population of monocytes differentiating into macrophages that was enriched in BAL samples from smokers with chronic obstructive pulmonary disease (COPD). Our smoking-associated airspace monocytes strongly and specifically expressed markers found in the population of differentiating monocytes identified in Baßler *et al.* (*19*), further supporting that airspace monocytes accumulate in smokers and may serve as precursors to other tissue macrophage states (fig. S4, B to D). This prior work likewise found that COPD-linked differentiating monocytes exhibited associations with smoking and elevated expression of lipid metabolism genes, both of which were concordant with our dataset and reflected through compositional analyses [Fig. 1B for flow cytometry compositional analyses; fig. S2 (D and E) for scRNA-seq compositional analyses], gene expression analyses (fig. S4, A to D), and histological staining of BAL cells for neutral lipids (fig. S4, E and F). Phenotypic gene modules linked to these disease-associated monocytes (such as infiltration/differentiation and lipid dysregulation) were up-regulated in airspace monocytes from smokers compared with those from never smokers in our dataset, further supporting the link between smoking and perturbed monocyte states (fig. S4C). As a control, we confirmed that the differentiating monocyte phenotype was not correlated with potential cohort structure confounders, such as age or biological sex, but was correlated with other previously published smoking-related gene sets in airspace immune cells (figs. S3, D to F, and S4G). In line with our analyses of smokers in the HLCA, we likewise found a positive trend between the proportion of

Downloaded from https://www.science.org at Massachusetts Institute of Technology on December 07, 2023

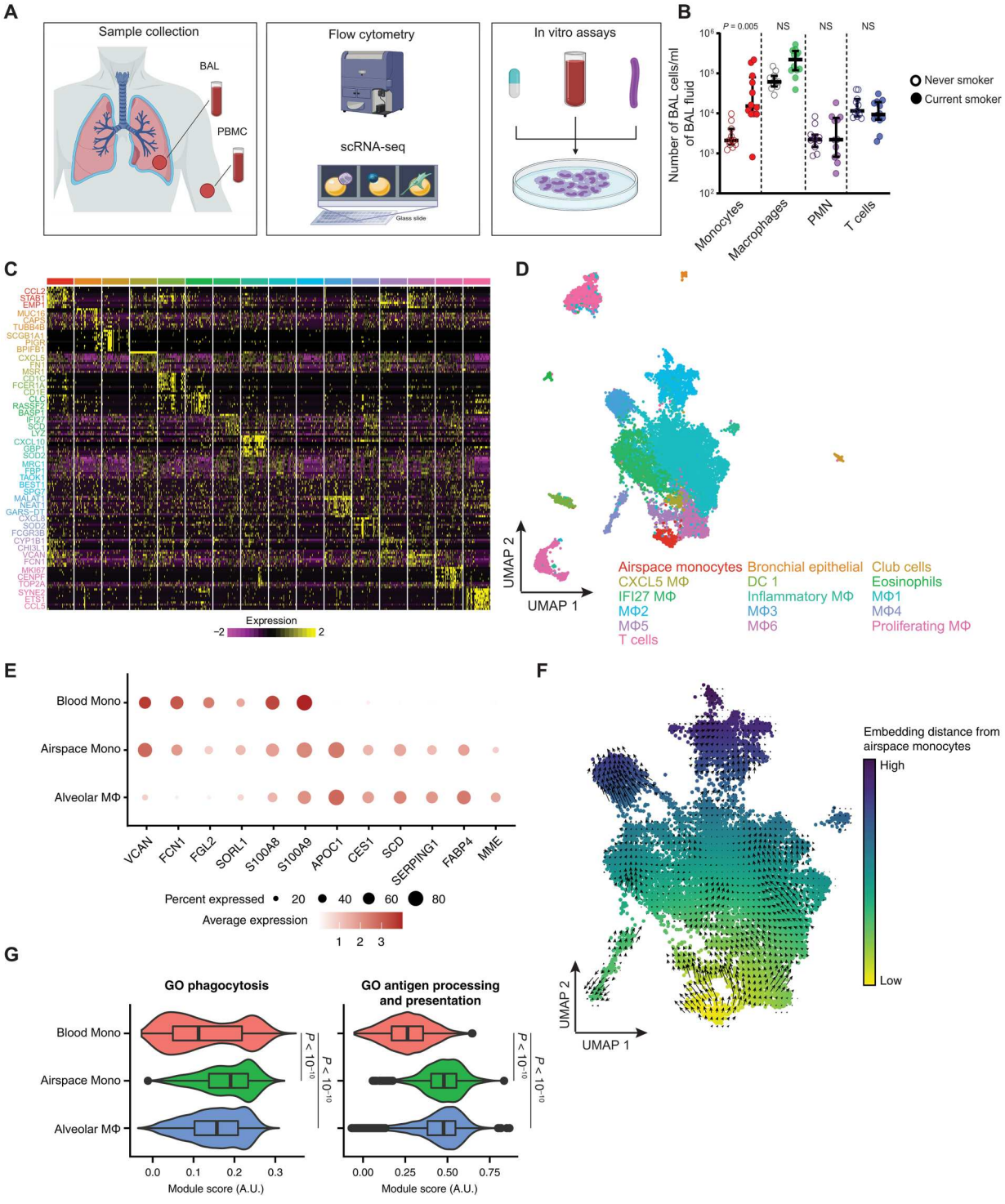

Fig. 1. Numbers of differentiating airspace monocytes are increased in the lungs of tobacco smokers. (**A**) Schematic of the sample processing pipeline using Seq-Well S^3, flow cytometry, and in vitro assays. (**B**) Analysis of the total number of viable cells/ml of BAL fluid in nonsmokers versus smokers. A scatter plot is labeled with median and interquartile range. *P* values were determined by a nonparametric one-way ANOVA and Dunn's multiple comparisons test. $n = 11$ nonsmokers, $n = 12$ smokers. (**C**) Heatmap showing normalized gene expression values [log (scaled UMI + 1)] for cell type–defining genes. (**D**) Uniform Manifold Approximation and Project (UMAP) plot ($n = 20{,}799$ cells; $n = 4$ nonsmokers, 5 smokers) colored by cell types. MΦ, macrophage; DC, dendritic cell. (**E**) Dot plot of myeloid-associated marker genes that distinguish blood monocytes and macrophages, with airspace monocytes exhibiting an intermediate phenotype. (**F**) RNA velocity analysis of differentiation trajectories among myeloid cells derived from BAL samples, colored by distance in embedding space from airspace monocyte cluster. (**G**) Module scoring for Gene Ontology (GO) processes relevant to monocyte/macrophage function. $P < 0.001$ by Wilcoxon rank sum test with Benjamini-Hochberg (B.H.) correction for multiple hypothesis testing. Box-and-whiskers plot has a box indicating median and interquartile range, and whiskers extending to the data point not further than the 1.5× interquartile range. NS, not significant.

Downloaded from https://www.science.org at Massachusetts Institute of Technology on December 07, 2023

airspace monocytes and the number of cigarette pack-years in our dataset (fig. S4H) (*20*–*23*).

In summary, we used flow cytometry and scRNA-seq to identify an airspace monocyte population that is preferentially enriched in the airspaces of tobacco smokers and exhibits phenotypes intermediate between circulating blood monocytes and more mature macrophages in the airspaces. RNA velocity analyses supported these airspace monocytes as progenitors for other macrophage subpopulations that are also enriched in smokers, and comparison with prior studies revealed concordant up-regulation of genes observed in disease-associated monocyte phenotypes.

Airspace monocytes originate from blood monocytes and share the expression of CD93

To further characterize the airspace monocytes enriched in smokers, we compared gene signatures of airspaces versus blood monocytes from the same donors. Differential expression and gene set enrichment analysis (GSEA) revealed enrichment in airspace monocytes for pathways associated with immune activation, up-regulation of defense mechanisms, and locomotion (Fig. 2, A and B, and fig. S5) compared with blood monocytes. To better understand connections between airspace and blood monocytes, we used pseudo-time analyses to find a trajectory that preserves the high-dimensional structure of our scRNA-seq dataset while ordering cells according to smooth gradients in gene expression (*24*). Complementing the orthogonal RNA velocity analyses (Fig. 1F), these results suggested that airspace monocytes originate from blood monocytes and assume intermediate positions along the differentiation trajectory toward more mature macrophage states (Fig. 2C). They also revealed genes that vary with smoking-associated recruitment, infiltration, and differentiation, such as (i) genes elevated early in pseudo-time (those associated with blood monocytes) but rapidly lost with differentiation (e.g., signaling receptors like *CSF3R*, *CX3CR1*, and *CXCR4*; inflammation-associated genes like *F13A1*, *DUSP1*, and *CTSS*), (ii) genes that were elevated at intermediate stages of the pseudo-time continuum from monocyte to macrophage (e.g., secreted proteins like *CTSL* and *C1QA*; cell surface–related genes like *CD81*, *DST*, and *DAB2*), and (iii) markers of mature macrophages that only increase at the terminus of the pseudo-time ordering (e.g., *CD163*, *FCGRT*, and *CD68*) (Fig. 2D).

To further investigate links between blood and airspace monocytes, we focused on the marker genes common to airspace and blood monocytes, thereby producing a gene signature that distinguishes monocytes in each compartment from mature AMs and MDMs. When we intersected airspace monocyte marker genes, blood monocyte marker genes, genes used to order the pseudo-time trajectory, and marker genes from two bulk RNA-seq datasets of smoking-induced airway changes (*25*, *26*), we found that *CD93* was the only gene that was shared independent of compartment, smoking status, analysis type, or dataset (Fig. 2E). In our cohort and the HLCA dataset, we found that *CD93* was expressed in blood and airspace monocytes but only sparsely detected by scRNA-seq in other myeloid cell types (Fig. 2F and fig. S6A). Concordantly, *CD93* was among the genes highest in blood monocytes and decreased with progression along the pseudo-time trajectory toward mature macrophage states (Fig. 2D). These data support airspace monocytes as a population derived from blood monocytes, infiltrating the airspaces in smokers, expressing CD93, and exhibiting an intermediate phenotype consistent with differentiation toward MDMs.

We next confirmed CD93 as a marker capable of identifying immature newly recruited monocytes in the airspaces at the protein level using flow cytometry. CD93 was not expressed by AMs but was expressed by 50% (median) of airspace monocytes, whereas 100% (median) of blood monocytes were positive for CD93 independent of smoking status (Fig. 3A and fig. S6B). Given that CD14 and CD16 mark canonical blood and alveolar myeloid populations (CD14 as highly expressed in conventional blood monocytes but decreased in mature AMs; CD16 as only expressed on subsets of unconventional $CD14^{+/low}$ blood monocytes but highly expressed by mature AMs), we sought to evaluate how CD93 associated with these subtype- and maturation-linked markers (*27*–*29*). In contrast to CD93, CD16 was expressed by a small fraction of blood monocytes (median 9%), with a higher proportion of airspace monocytes (median 75%) and all AMs (median 95%) (Fig. 3B). $CD93^{+}$ airspace monocytes showed higher expression of *CD14* mRNA (associated with circulating blood monocytes) but lower expression of CD16 protein (otherwise associated with mature AMs) than did $CD93^{-}$ airspace monocytes (fig. S6, C and D). Thus, our data indicate that the airspace monocyte–identifying marker CD93 was down-regulated or shed early during maturation while other myeloid maturation–associated markers, such as CD16 and CD14, were up- or down-regulated, respectively. To more directly explore the expression of this marker during maturation, we isolated blood monocytes and followed CD93, CD16, and CD14 over a maturation period in human serum of 9 days in vitro. Monocytes increased in size and granularity (SSC versus FSC), indicating their maturation state at different time points (Fig. 3C). CD93 expression decreased by 2 hours after adherence of blood monocytes and was almost undetectable after 24 hours of maturation (Fig. 3D), while CD16 was significantly ($P = 0.0001$) up-regulated during the same time (Fig. 3E); CD14 remained approximately constant (Fig. 3F). We further sought to leverage our scRNA-seq atlases to demonstrate that CD93 enables additional specificity compared with the canonical myeloid markers of CD14 and CD16. In contrast to the specificity of CD93 for marking airspace monocytes among cells isolated through BAL and linking them to blood monocytes (Fig. 2F), a variety of macrophage subsets showed slightly lower expression of *CD14* than did airspace monocytes (fig. S6E), and airspace monocytes' expression of *FCGR3A* (encoding CD16) was not substantially different in mature macrophage subsets (fig. S6F). Thus, CD93 identifies an enriched monocyte population in the airspace of smokers, beyond the canonical myeloid markers of CD14 and CD16.

In summary, airspace monocytes exhibit phenotypes intermediate between immature blood monocytes and mature macrophages. We identified CD93 as a unique marker for blood and airspace monocytes that is rapidly lost as airspace monocytes mature into macrophages and express markers including CD16 but provides additional specificity for delineating airspace monocytes from more mature macrophages in the alveolar environment. Therefore, $CD14^{+}CD93^{+}CD16^{-/low}$ airspace monocytes represent a cluster of undifferentiated, recently transmigrated blood-derived monocytes that are enriched in the lungs of tobacco smokers.

Downloaded from https://www.science.org at Massachusetts Institute of Technology on December 07, 2023

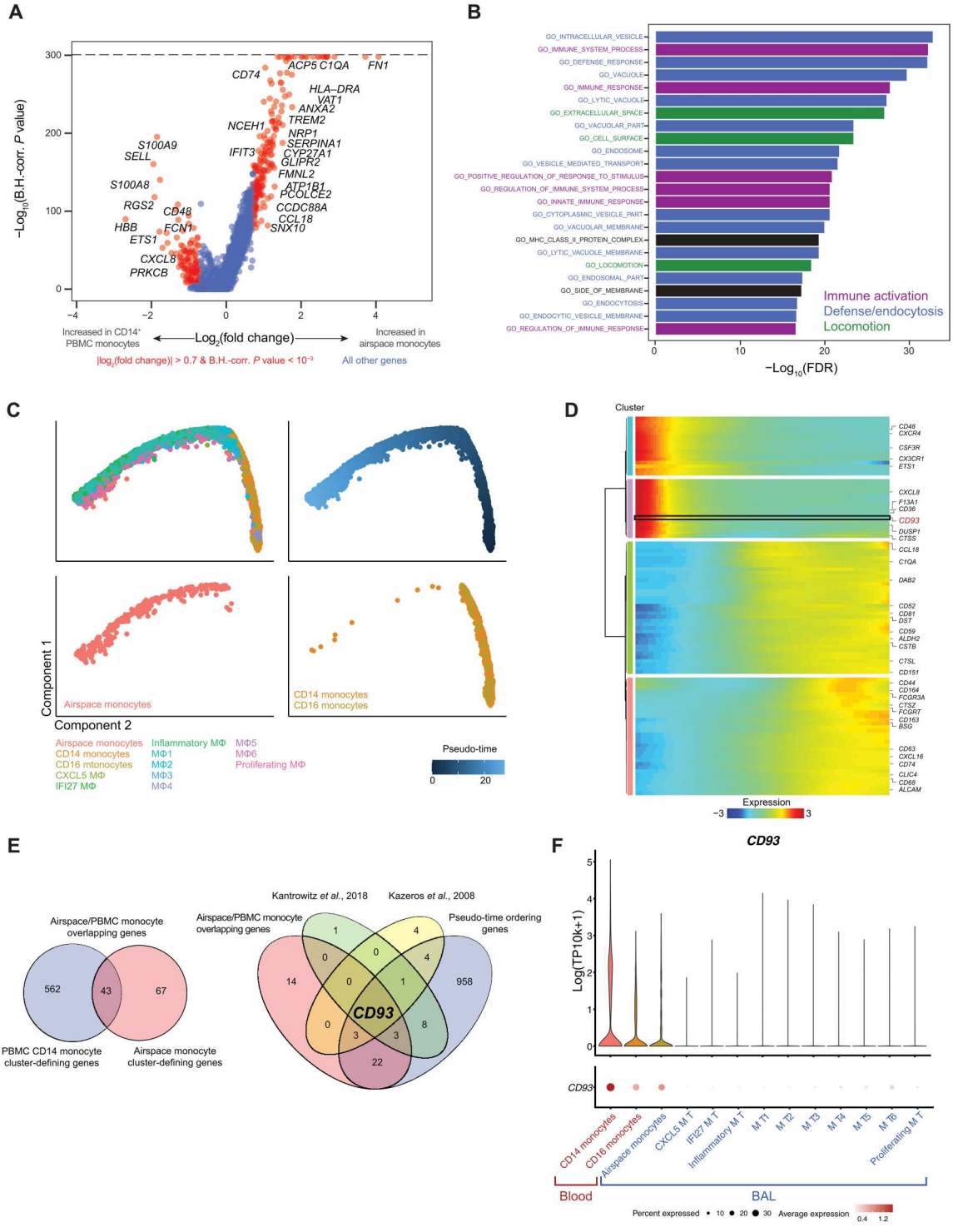

Fig. 2. Airspace monocytes are distinct from blood monocytes but share the identifying marker CD93. (**A**) Volcano plot of differentially expressed genes between airspace monocytes and CD14$^+$ PBMC monocytes. The *x* axis represents airspace-vs-CD14$^+$ monocyte fold change in expression (positive = increased in airspace monocytes; negative = increased in CD14$^+$ PBMC monocytes), and the *y* axis represents B.H.-corrected *P* values. Red indicates genes with $|\log_2(\text{fold change})| > 0.7$, and blue indicates all other genes. (**B**) Bar plot of gene programs enriched in airspace monocytes identified from GO enrichment analysis. FDR, false discovery rate. (**C**) Pseudo-time trajectory analysis of myeloid-lineage cell types from both blood and lung, colored by cell type (top left, bottom left, and bottom right) or pseudo-time coordinate (top right). (**D**) Heatmap of top genes differentially expressed along the pseudo-time trajectory. (**E**) Left: Venn diagram of the number and overlap of genes between airspace monocyte and CD14$^+$ PBMC monocyte cell type–defining genes. Right: Venn diagram of the number and overlap of gene analyses in four datasets. (**F**) Violin plot and dot plot of *CD93* expression across myeloid clusters; TP10k = transcripts per 10,000.

Downloaded from https://www.science.org at Massachusetts Institute of Technology on December 07, 2023

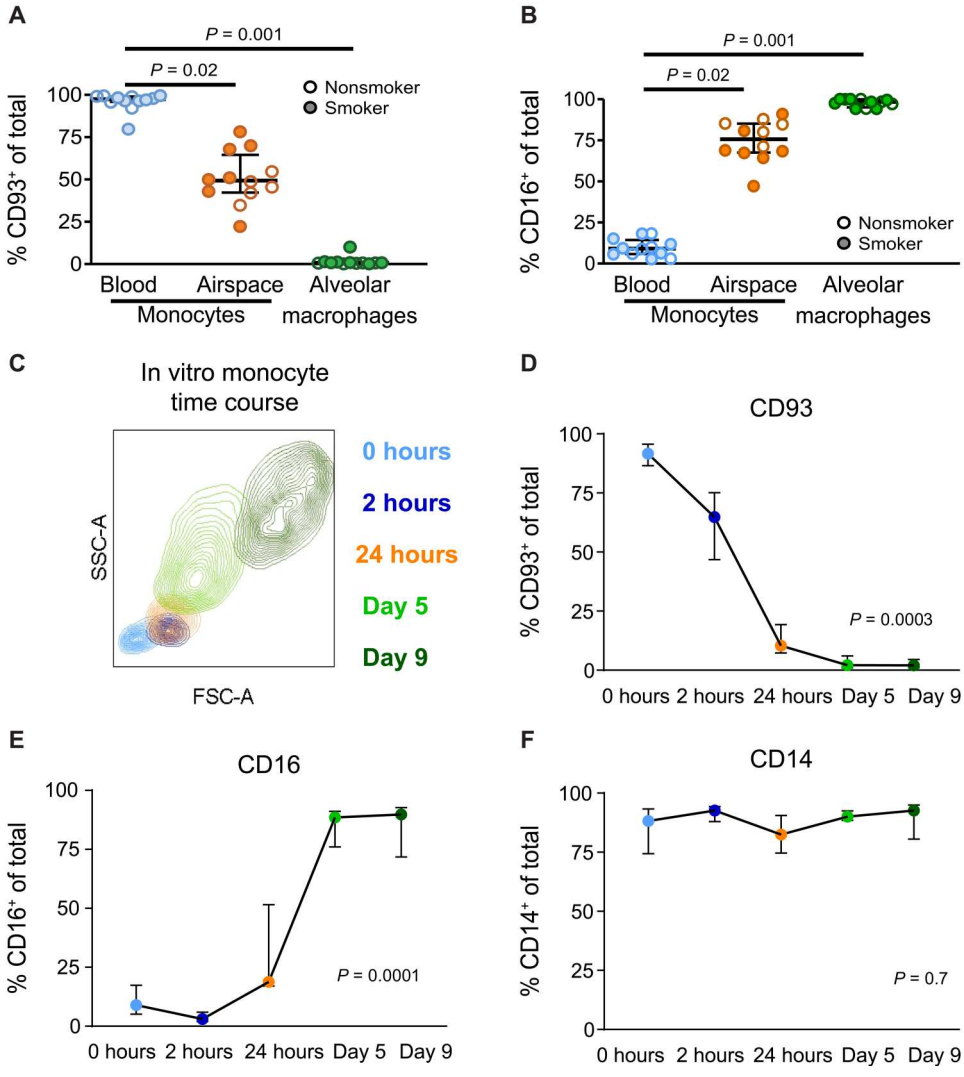

Fig. 3. CD93 and CD16 reflect different stages of monocyte maturation in vivo and in vitro. (**A** and **B**) Blood monocytes, airspace monocytes, and alveolar macrophages were identified as shown in Fig. 1 and analyzed for the frequency of CD93$^+$ (A) and CD16$^+$ (B) subsets using flow cytometry (n = 5 nonsmokers, n = 7 smokers). (**C** to **F**) Blood monocytes were isolated from the PBMCs of nonsmokers (n = 6) and differentiated into MDMs in vitro. MDMs were analyzed for forward and side scatter distributions (C), as well as the frequency of cells positive for CD93 (D), CD16 (E), and CD14 (F) at different time points using flow cytometry. P values were determined by (A and B) Kruskal-Wallis and Dunn's multiple comparisons tests or (D to F) Friedman test, showing median with interquartile ranges.

Monocytes are recruited to the airspaces through CCR2-binding chemokines

Our analysis of myeloid cells revealed that tobacco smoking induces an accumulation of CD93$^+$ airspace monocytes. Circulating monocytes expressed the chemokine receptor CCR2 and up-regulate CCR5 upon transmigration and activation (*30*). To investigate the chemokines that recruit circulating monocytes into the airspaces, we measured 15 chemokines along with 10 cytokines in BAL fluid from smokers and never smokers. We found positive correlations between the number of airspace monocytes and CCR2- and CCR3-binding chemokines (CCL2 and CCL7 as binding to CCR2; CCL11 as binding to both CCR2 and CCR3; Fig. 4A and fig. S7, A to F). Although *CCR3* was only sparsely detected in scRNA-seq data, *CCR2* and *CCR5* were both up-regulated in airspace monocytes from smokers as compared with never smokers, but not in blood monocytes (Fig. 4, B and C, and fig. S7G). Because CCL11 exhibited the strongest correlation with airspace monocyte abundance in BAL, we proceeded to experimentally evaluate CCL11's effects on monocyte migration in vitro. We found that recombinant CCL11 was sufficient to attract monocytes in a CCR2-dependent manner in vitro (Fig. 4D and fig. S7H); this CCR2-dependent transmigration was specific to monocytes and was not observed for CD4$^+$ or CD8$^+$ T cells. In addition, when treating BAL fluid from smokers with a blocking antibody against CCL11, transmigration of blood monocytes was significantly (P = 0.02) reduced, whereas a CCL2-blocking antibody did not produce a significant (P = 0.4) effect (Fig. 4E). Thus, the smoking-associated recruitment of monocytes to the airspaces correlates with well-known monocyte chemo-attractants like CCL2 and CCL7 but also CCL11, a chemokine whose effects on monocytes had been previously incompletely explored in this context.

Downloaded from https://www.science.org at Massachusetts Institute of Technology on December 07, 2023

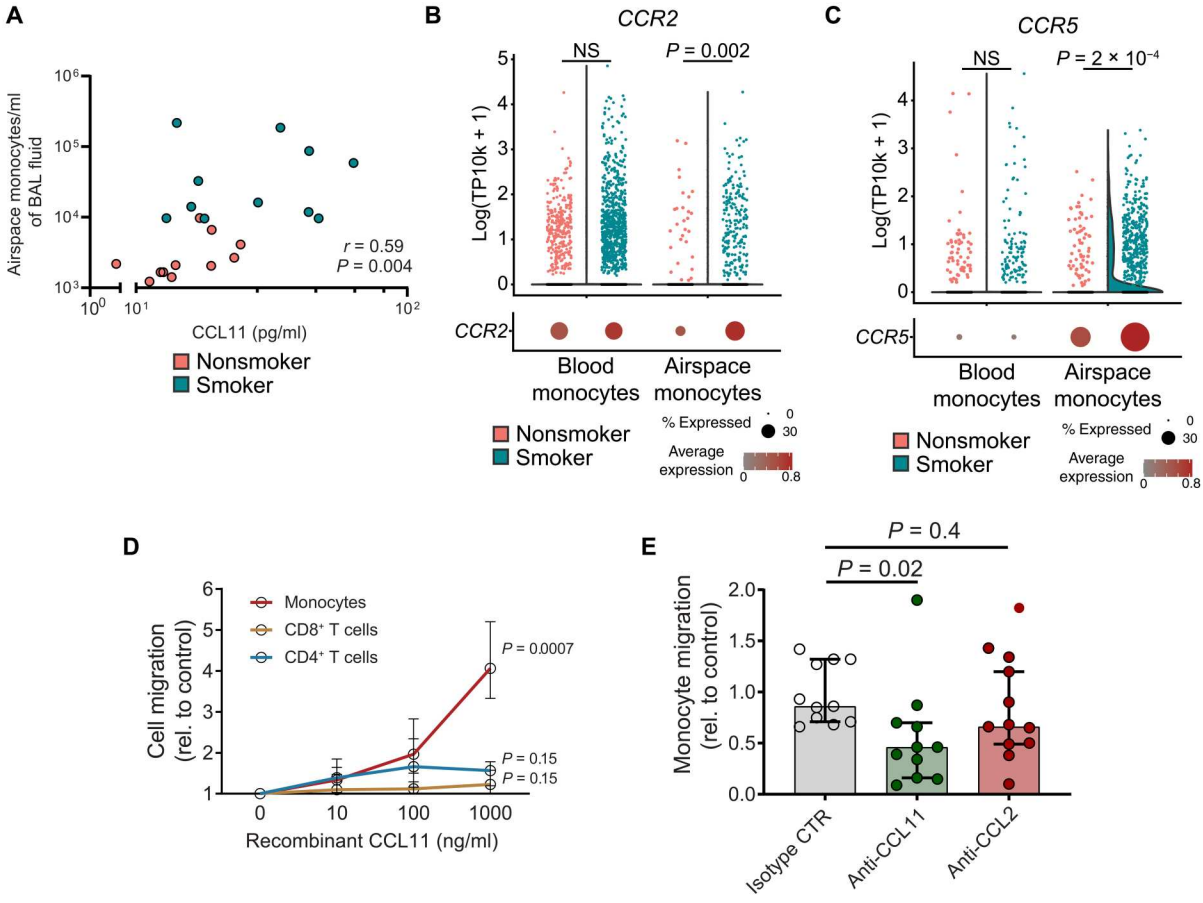

Fig. 4. Nonclassical chemokines recruit monocytes into the BAL of tobacco smokers. (**A**) BAL fluid from smokers and nonsmokers was concentrated (30×), and 15 chemokines were measured using a multiplex system. CCL11 concentration in BAL fluid of smokers (turquoise circles) and nonsmokers (salmon circles) was correlated with the number of airspace monocytes per ml of BAL fluid using Spearman's nonparametric test ($N = 11$ nonsmokers, $N = 11$ smokers). (**B** and **C**) Violin plot and dot plot of expression of the chemokine receptors *CCR2* (B) and *CCR5* (C) on airspace or blood monocytes from smokers (turquoise) or nonsmokers (salmon). (**D** and **E**) The indicated cell types were layered on top of a 3-μm Transwell to monitor monocyte migration toward media containing different concentrations of recombinant CCL11 ($n = 5$) (D) or concentrated BAL fluid from smokers ($n = 11$) incubated with an isotype control antibody, antibodies against CCL11, or antibodies against CCL2 (E). rel., relative. Statistical significance was evaluated by (A) Spearman's correlation, (B and C) Wilcoxon rank sum test with B.H. correction for multiple hypothesis testing, or (D and E) Kruskal-Wallis and Dunn's multiple comparisons tests showing median with interquartile ranges.

Airspace and blood monocytes respond to *Mtb* with a strong inflammatory response compared with AMs

Monocytes can drive acute and chronic tissue inflammation, with an elevated inflammatory capacity as compared with that of macrophages (*31*). In a mouse model of human TB, uncontrolled infiltration of monocytes into the lung during infection was associated with increased pathology and susceptibility to accelerated *Mtb* growth (*32*). Furthermore, the release of pro-inflammatory interleukin-1β (IL-1β) is facilitated by an alternative pathway of inflammasome activation that has been shown to be active in monocytes but not in differentiated macrophages (*33*). Thus, we hypothesized that, in the context of *Mtb* exposure, smoking-mediated recruitment of monocytes to the airspaces may result in an increased inflammatory milieu and a host lung microenvironment amenable to bacterial seeding and persistence. Compared with AMs, airspace monocytes were enriched for pathways associated with immune activation, chemokine production, and chemotaxis, suggesting that they have high inflammatory potential and may contribute to an accelerated inflammatory response in the lungs during infection (Fig. 5A). Pro-inflammatory transcriptional signatures were further enhanced in airspace monocytes from smokers versus nonsmokers at the single-cell level, suggesting both smoking-mediated recruitment and cell-intrinsic changes (fig. S7, I and J). Therefore, we examined whether monocytes and macrophages would respond differently in vitro when exposed to *Mtb* or Toll-like receptor (TLR) ligands. Blood monocytes released IL-1β and other pro-inflammatory chemokines (e.g., CCL3 and CCL4) and cytokines [e.g., tumor necrosis factor–α (TNF-α) and IL-1α] after exposure to *Mtb* or TLR ligands, whereas MDMs and donor-matched AMs did not (Fig. 5, B and C; fig. S7, K to L; and tables S3 and S4). Adherent BAL cells from smokers, which contain about 10-fold higher counts of airspace monocytes as compared with BAL samples from never smokers (Fig. 1B), secreted higher amounts of IL-1β and other pro-inflammatory chemokines and cytokines after exposure to *Mtb* (fig. S7, M and N, and table S3). In contrast, BAL cells from never smokers largely did not produce a pro-inflammatory response after *Mtb* exposure. As a tractable experimental system to evaluate airspace monocytes' ability to increase inflammatory responses with *Mtb*

Downloaded from https://www.science.org at Massachusetts Institute of Technology on December 07, 2023

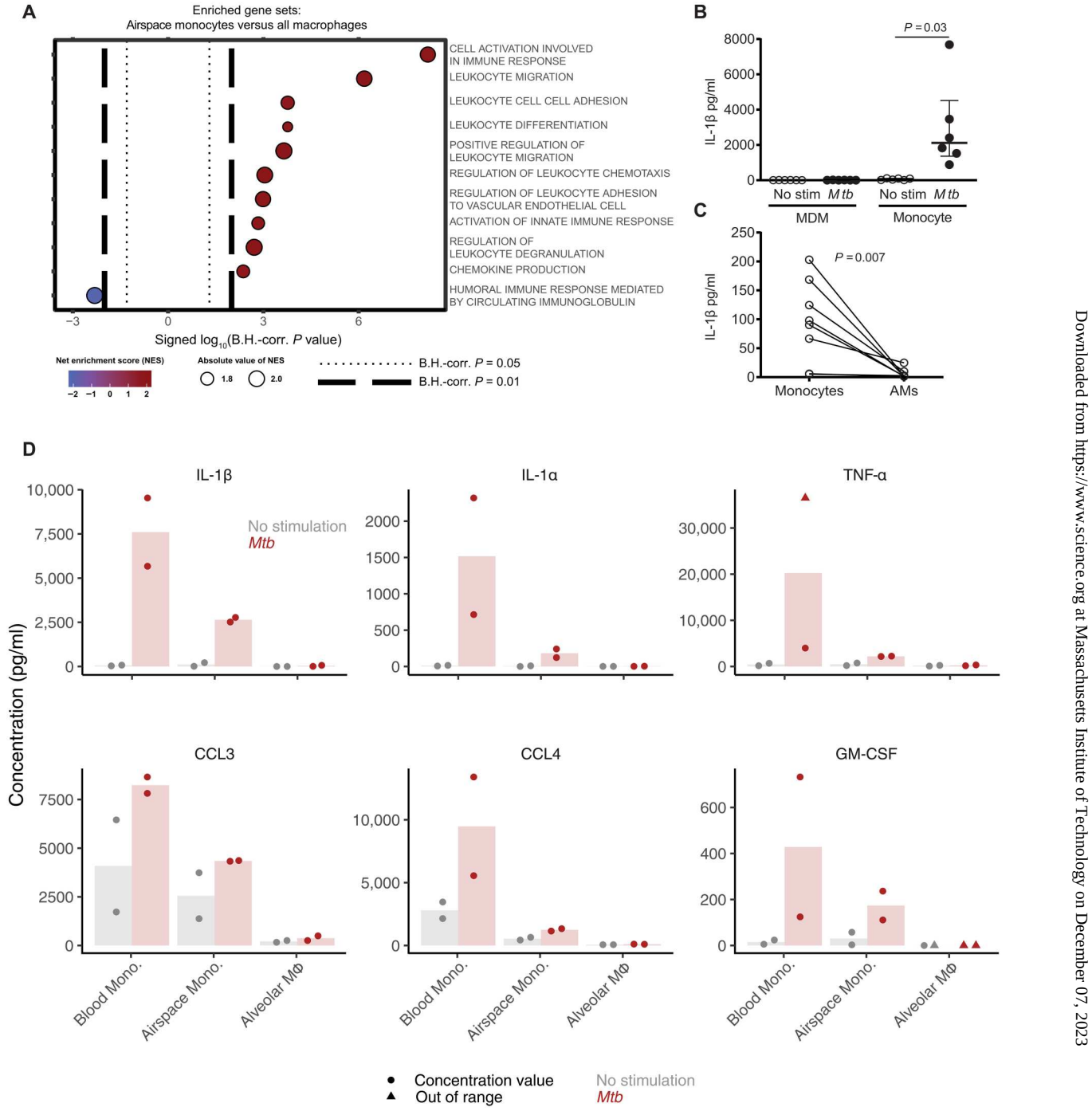

Fig. 5. Blood and airspace monocytes are highly pro-inflammatory compared with mature macrophages. (**A**) GO processes enriched in GSEA of differentially expressed genes between airspace monocytes and all macrophages. B.H. correction was applied to *P* values from GSEA to control for multiple hypothesis testing. Dotted lines indicated B.H.-corrected $P = 0.05$; dashed lines indicate B.H.-corrected $P = 0.01$. (**B**) IL-1β concentrations were measured in MDMs and blood monocytes with or without 24 hours of *Mtb* exposure ($n = 6$). (**C**) IL-1β concentrations were measured in donor-matched blood monocytes versus BAL macrophages from nonsmokers upon stimulation with *Mtb* ($n = 8$). (**D**) Cytokine concentrations are shown for donor-matched sorted blood monocytes, airspace monocytes, and BAL macrophages across two smokers. In (B) to (D), each dot represents a sample from a different participant. The *P* values were measured by (B) Friedman test and Dunn's multiple comparisons, showing a median with interquartile ranges, or (C) by a two-sided Wilcoxon test.

Downloaded from https://www.science.org at Massachusetts Institute of Technology on December 07, 2023

infection in the context of smoking-induced microenvironments, we cultured monocytes and MDMs with cigarette smoking extract (CSE), followed by exposure to *Mtb*. In line with the ex vivo observations, monocytes but not MDMs up-regulated transcription of IL-1β upon exposure to *Mtb* in the presence of CSE ($P = 0.02$ for monocytes, $P = 0.90$ for MDMs; fig. S7O). These results provide functional support for the pro-inflammatory transcriptional signatures observed in airspace monocytes and highlight how smoking may prime the lung immune environment for amplified inflammatory responses after pathogen challenge. Toward illustrative demonstrations of cell type–specific differences in inflammatory responses, we sorted airspace monocytes and AMs, obtaining sufficient airspace monocytes and AMs from two donors for comparisons against donor-matched purified blood monocytes. Whereas AMs showed undetectable or low production of inflammatory cytokines after exposure to *Mtb*, both matched airspace monocytes and blood monocytes secreted pro-inflammatory IL-1β and other inflammatory markers and cytokines (e.g., IL-1α and TNF-α), chemokines (e.g., CCL3 and CCL4), and growth factors (e.g., GM-CSF) upon *Mtb* stimulation, with airspace monocytes exhibiting intermediate secretion between those of macrophages and blood monocytes (Fig. 5D and tables S4 and S5). These results indicate that airspace monocytes have a heightened inflammatory phenotype after transmigration from the blood into the tissue and respond with an exuberant inflammatory response after lung exposure to *Mtb*.

Monocyte inflammatory responses drive their susceptibility to *Mtb* growth

The accumulation of monocytes at the site of infection has been associated with increased susceptibility to *Mtb* growth in murine and zebrafish models (*34*). Hence, the specific contribution of smoking to the recruitment and enrichment of human airspace monocytes may represent a mechanism of accelerated growth of *Mtb*, thereby driving active TB in humans. However, direct links between tobacco-associated increases in airspace monocytes and *Mtb* intracellular growth have not been established. We found that *Mtb* growth was significantly ($P = 0.0001$) increased in monocytes compared with mature MDMs (Fig. 6A) or AMs (Fig. 6B), but this intracellular growth was not associated with increased *Mtb*-induced cell death in vitro (fig. S8A). Adherent BAL cells from smokers, which contain a higher frequency of monocytes, showed high permissiveness to *Mtb* intracellular growth (fig. S8B), suggesting that BAL and blood monocytes are highly susceptible to intracellular *Mtb* growth.

Our in vitro colony-forming unit (CFU) data were further supported by a reanalysis of scRNA-seq data from *Mtb* granulomas in a macaque model that recapitulates the diversity of outcomes observed in human disease (*35*). On the basis of both a module of airspace monocyte markers and *CD93* specifically, we identified a cluster of macaque myeloid cells with similar expression features to human airspace monocytes (fig. S8, C and D). We labeled this cluster "airspace monocyte–like" cells and proceeded to quantify their potential disease relevance. We examined how the expression of canonical inflammatory genes changed with smoking (in human airspace monocytes) and tuberculosis burden (in macaque airspace monocyte–like cells from *Mtb* granulomas). Of the 36 hallmark inflammatory response genes with statistical significance and detection in >10% of cells in both datasets (200 genes in inflammatory response gene set), 32 genes were both up-regulated with smoking and positively associated with bacterial burden, including *IL1B* and *CD14* (Fig. 6C). This suggests that the same genes up-regulated in human airspace monocytes with smoking are linked to elevated *Mtb* burden in macaque granulomas, connecting smoking, monocytes' inflammatory phenotypes, and *Mtb* burden.

Next, we investigated whether inflammatory monocyte states are specifically associated with increased susceptibility to *Mtb* growth. Monocytes and MDMs were treated with dexamethasone or the anti-inflammatory small molecule inhibitor SP600125 (Jun N-terminal kinase inhibitor). As expected, both inhibitors reduced inflammatory cytokine production by monocytes after *Mtb* exposure (fig. S9, A and B); however, they also inhibited *Mtb* intracellular growth specifically in monocytes (Fig. 6, D and E, and fig. S9, C and D), supporting the role of pro-inflammatory monocytes in promoting *Mtb* growth. Inhibition of inflammasome activation alone was not sufficient to reduce *Mtb* intracellular growth (fig. S9, E and F), suggesting that dexamethasone and SP600125 treatment might work through different inflammatory pathways or mechanisms, such as changes in metabolic activity. Pro-inflammatory responses and enhanced antimycobacterial effector mechanisms have previously been associated with increased glycolysis by mature macrophages (*36*–*38*). At a transcriptional level, blood monocytes exhibited lower expression of genes involved in glycolysis than AMs (fig. S9G). In a functional assay, monocyte L-lactate production (a proxy for glycolytic activity) (*39*) was significantly lower after stimulation with *Mtb* or *Mtb* plus dexamethasone than observed with lipopolysaccharide (LPS) stimulation ($P = 0.04$; fig. S9H), whereas in MDMs, *Mtb* and LPS enhanced L-lactate production (fig. S9I). This indicates that the glycolytic activity and antimycobacterial effector mechanisms of monocytes are differentially regulated compared with macrophages, paralleling their differential *Mtb* susceptibility and inflammatory responses.

Building on our observation that tobacco smoking drives increased recruitment of inflammatory immature monocytes to the airspaces, we found that the pro-inflammatory phenotype of these monocytes enables accelerated intracellular growth of *Mtb*, which can be abrogated through anti-inflammatory small molecule treatment in vitro. In addition, we observed decreases in monocyte glycolysis after *Mtb* stimulation that may contribute to decreased antimycobacterial activity. Thus, inflammatory immature airspace monocytes may represent a *Mtb*-permissive subpopulation that underlies the increased risk for active TB associated with smoking.

DISCUSSION

Smoking has long been linked as a strong risk factor for active TB, yet the specific mechanisms underlying this observation remain incompletely understood (*5*). In this work, we performed a high-resolution analysis of lung immune cell composition, dynamics, and phenotypes in smokers to understand how tobacco smoking perturbs the lung microenvironment to promote increased *Mtb* growth. In our study, smoking was associated with the enrichment of immature inflammatory airspace monocytes that likely were derived from newly recruited blood monocytes. We identified CD93 as a marker capable of distinguishing these immature airspace monocytes from more mature $CD16^+$ airspace monocytes, AMs, or MDMs and provided evidence that CCL11, among other CCR2-binding chemokines, was an important chemoattractant involved in the specific recruitment of monocytes to the airspaces of

Downloaded from https://www.science.org at Massachusetts Institute of Technology on December 07, 2023

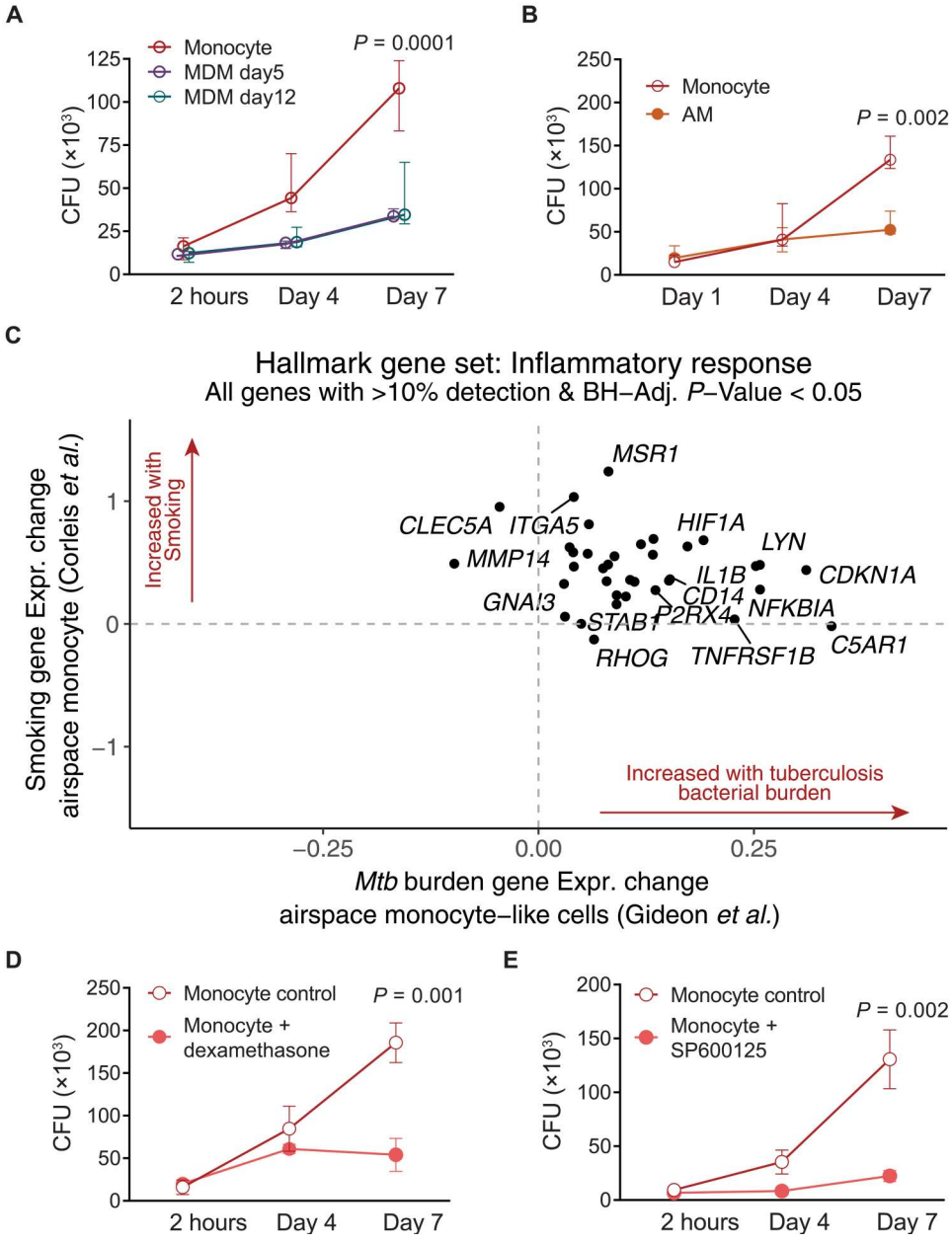

Fig. 6. An elevated monocyte inflammatory response is associated with increased intracellular growth of *Mtb*. (**A**) Monocytes were isolated from human PBMCs (n = 6 or 7) and infected with *Mtb* H37Rv at a MOI of 0.1 or differentiated for 5 or 12 days (into MDMs) before infection with *Mtb* H37Rv. At indicated time points, macrophages were lysed to release intracellular bacteria, and the number of intracellular bacteria was determined by counting CFUs. MDM samples were slightly offset in the x direction to aid with visualization. (**B**) AMs from nonsmokers or donor-matched monocytes (N = 4) were infected with *Mtb* H37Rv and CFUs were quantified as described in (A). (**C**) Expression (Expr.) changes of hallmark inflammatory response genes with bacterial burden in granulomas and smoking; all hallmark inflammatory response genes detected in >10% of cells and with statistical significance are shown [Mann-Whitney U test with B.H. correction across all tested genes (B.H.-adjusted or adj.) for human airspace monocytes with smoking; limma trend with B.H. correction across all tested genes was used for association with *Mtb* burden in macaque airspace monocyte–like cells]. (**D** and **E**) Monocytes (N = 3) were infected as described in (A). Where indicated, dexamethasone (D) or SP600125 (E) was added directly after 2 hours for the remaining time course. The P values were calculated by Friedman test and Dunn's multiple comparisons test for each time point, showing a median with interquartile ranges.

Downloaded from https://www.science.org at Massachusetts Institute of Technology on December 07, 2023

smokers. Before *Mtb* exposure, airspace monocytes from smokers exhibited higher expression of inflammation- and activation-linked gene modules than did AMs. Consistent with this, BAL cells from smokers produced elevated inflammatory responses after *Mtb* exposure as compared with cells from never smokers, supporting the conclusion that smoking primes pro-inflammatory lung environments and immune responses. This increased inflammatory state was associated with enhanced *Mtb* growth in vitro, which could be inhibited by treatment with anti-inflammatory drugs (e.g., dexamethasone) specifically in monocytes but not in macrophages, further supporting ties between smoking-induced immature inflammatory monocyte populations/states and susceptibility to *Mtb*. Overall, our data demonstrate that the increased recruitment and presence of immature inflammatory airspace monocytes in the lungs of smokers may contribute to their increased risk of active TB.

We observed an increased number of total BAL cells in smokers that was primarily explained by the infiltration of $CD14^+$ monocytes. An increased number of myeloid cells in the airspaces of smokers has been reported before (*40*–*42*). However, in those studies, myeloid cells were identified using methods that did not discriminate between monocyte and macrophage subpopulations. One study found a decrease in CD16 expression and a slight increase in CD14 expression on the surface of BAL cells from smokers and patients with COPD, consistent with the $CD14^+$ monocyte phenotype in our cohort (*41*). Using scRNA-seq, characterization of airspace monocytes that differentiate further into a number of macrophage phenotypes has also been described in patients with coronavirus disease 2019 (COVID-19) and COPD, confirming the connection between inflammation, disease, and recruited monocytes across multiple lung disorders (*19*, *43*, *44*, *45*). We specifically identified CD93 as a marker for defining a disease-relevant population of airspace monocytes, enriched in smokers′ airspaces. Initially, CD93 was found as a receptor for the complement factor C1q, which is enhanced in patients with TB. However, more recent data were not able to confirm the binding of C1q to CD93, suggesting instead a role in migration and adhesion (*46*, *47*). We demonstrated that CD93 enabled more specific identification of pro-inflammatory airspace monocytes as compared with canonical myeloid markers. Thus, $CD14^+CD93^+CD16^{low}$ monocytes in the airspaces represented a transcriptional and functional intermediate state between $CD93^+$ blood monocytes and AMs, with $CD93^+$ airspace monocytes retaining pro-inflammatory phenotypic characteristics of blood monocytes, despite translocation into the tissue microenvironment. Examination of myeloid-associated disease-linked gene sets, RNA velocity, and pseudo-time analyses all supported the observation that airspace monocytes differentiate toward more mature macrophage states. Furthermore, ex vivo *Mtb* exposure assays demonstrated that the protein-level functional responses of airspace monocytes were capable of driving inflammation in the airspaces. Thus, our work demonstrates smoking-mediated recruitment of immature inflammatory monocytes that retain functional characteristics of blood monocytes despite ongoing differentiation, thereby establishing a lung niche conducive to elevated *Mtb* growth. Toward further understanding smoking-induced lung niches, our analyses of the HLCA identified interstitial macrophages as not only enriched with smoking but also present in former and active smokers, both of which were higher than never smokers. Future work should investigate the potential persistence of interstitial macrophages after smoking-mediated recruitment and differentiation of airspace monocytes and their relevance to TB.

Our data highlighted CCL11-CCR2 signaling as important for driving monocyte migration (with additional chemokines also being correlated with airspace monocyte counts). CCL11 is best known in the context of allergic asthma and eosinophil recruitment through CCR3 (*48*). However, it can also bind CCR2 (*49*), which is highly expressed on blood monocytes (*50*) and may facilitate myeloid cell recruitment, which had previously been shown in atopy (*51*), suggesting pleiotropic effects important in smoking-induced, airspace monocyte–linked *Mtb* susceptibility. In asthma, CCL11 requires a T helper 2 milieu and IL-5 for effective eosinophil recruitment (*52*). In our cohort of smokers, we did not detect a bias toward type 2 immune response and consequently did not observe any substantial increase in infiltration of eosinophils or neutrophils in airway samples. Instead, we detected an accumulation of pro-inflammatory airspace monocytes associated with signaling through chemokines binding CCR2. Building on these findings, future studies could evaluate shifts in chemokine concentrations in the air spaces and plasma in never smokers versus smokers.

Furthermore, we found a link between the pro-inflammatory phenotypes of airspace monocytes and increased *Mtb* growth, highlighting the importance of regulated, balanced immune responses for pathogen control. Innate immune activation and mobilization of hybrid type 1/type 17 adaptive immune responses are crucial for successful *Mtb* control (*35*); however, aberrant pro-inflammatory states can also be detrimental to the host (*53*, *54*). Prior work has suggested that elevated infiltration of immature inflammatory monocytes into the lung is associated with inflammation-induced tissue damage and higher susceptibility to *Mtb* (*32*, *55*, *56*). This model is further supported by findings demonstrating that highly pathogenic *Mtb* strains can drive increased pathology through elevated infiltration of monocytes (*34*). Glycolysis and pro-inflammatory macrophage responses are likewise associated with increased resistance to *Mtb* intracellular growth (*36*–*38*). Our studies in monocytes indicated a strong pro-inflammatory response to *Mtb* uncoupled from elevated glycolysis, warranting further investigation into the regulation of monocytes′ antimycobacterial effector mechanisms. One potential explanation is that high *IFNB* expression by *Mtb*-exposed monocytes might counteract other pro-inflammatory and antimycobacterial effector functions in these cells (*57*) to prevent activation of glycolytic pathways (*58*). Protective roles of pro-inflammatory immune responses in *Mtb* may depend on timing, location, and concentration of released signaling molecules, such that stronger inflammatory responses may not necessarily result in improved *Mtb* control. We found that treatment of monocytes with the anti-inflammatory molecules dexamethasone or SP600125 resulted in reduced *Mtb* intracellular growth. The two anti-inflammatory mediators used in this study have relatively broad mechanisms of action. Dexamethasone broadly inhibits inflammatory responses (among other suppressive effects on immune function as a glucocorticoid), whereas SP600125 acts as a Jun N-terminal kinase inhibitor. Given the effectiveness of both drugs in inhibiting *Mtb* growth in our ex vivo functional assays, their effects on *Mtb* growth would not seem to be inflammasome-dependent. We also note that dexamethasone and similar adjunctive glucocorticoids are already approved to reduce inflammation and increase survival in patients with TB-associated immune

Downloaded from https://www.science.org at Massachusetts Institute of Technology on December 07, 2023

reconstitution inflammatory syndrome and TB-associated meningitis (*59*, *60*). Our data suggest there may also be a benefit during the treatment of inflammatory diseases in tobacco smokers or patients with similarly pro-inflammatory lung environments.

A limitation of this study is its relatively small sample size. However, we provide support for the generalizability of our findings through comparisons against a variety of larger publicly available data. Future work could seek to replicate these results in additional cohorts and develop improved methods for highly efficient isolation of airspace monocytes. Toward this end, our analyses using previously published data on lung diseases and smoking revealed not only concordant phenotypes across diseases and cohorts but also that our findings are not driven by confounders related to cohort characteristics. Further meta-analyses leveraging published scRNA-seq datasets and mouse models of human disease (*61*) could enable broader inquiries into mechanisms of smoking as a risk factor for other pulmonary diseases through the identification of similar recruited human airspace monocyte populations. Likewise, although we demonstrated that smoking leads to increased recruitment of immature inflammatory monocytes to the airspaces and primes a niche for *Mtb* growth, further studies are needed to define more precise mechanisms of how these pro-inflammatory monocytes permit rapid *Mtb* growth. Future work could include direct studies on *Mtb* growth in primary airspace monocytes and molecular mechanisms of their permissiveness. However, we note that the isolation of airspace monocytes requires a high total volume of BAL. Out of a cohort of 12 study participants undergoing flow sorting of airspace monocytes, sufficient cell yield for downstream functional assays was only achieved in two smokers, motivating studies on peripheral blood monocytes (especially given experimental evidence and analyses supporting their status as putative progenitor cells of airspace monocytes).

Smoking has been reported to impair the ability of AMs to control *Mtb* intracellular growth (*6*, *9*, *11*). Our data suggest that the recruitment of immature inflammatory monocytes into the airspaces additionally provides a highly permissive cell type for *Mtb* growth that is also capable of inducing broader lung inflammation. Thus, our findings indicate that airspace monocytes provide an additional independent mechanism by which tobacco smoking increases the risk of *Mtb* acquisition and progression to active TB. Epidemiological studies have not fully elucidated whether smoking-associated active TB cases and TB mortality are due to increased risk of primary infection, reactivation, or reinfection. However, airspace monocytes could contribute to disease progression in a variety of ways. For instance, (i) LTBI presents as a spectrum, with active and sterilizing granulomas in the same lung parenchyma at the same time; here, collapsing granulomas could release mycobacteria, which might relocate to the airspaces for uptake by airspace monocytes (*62*, *63*); (ii) in endemic countries with high TB prevalence, reexposure and reinfection occur frequently and are common. Smoking-induced airspace monocytes might increase the risk of accelerated growth and dissemination of *Mtb* after repeated exposure (*64*, *65*, *66*); or (ii) indoor air pollution might trigger recruitment of airspace monocytes (similar to as here reported for active tobacco smoking). Indoor air pollution increases the risk of active TB in children, suggesting that the underlying mechanisms described may also be relevant to children exposed to indoor air pollution or second-hand smoking (*67*, *68*). Our work demonstrates how environmental exposures can drive the dysregulation of tissue microenvironments that, in turn, affect susceptibility to disease. In addition, we identify potential translational directions and specific small molecule approaches to modulate immune function for improved TB outcomes. These findings provide biological insight into the mechanism by which smoking increases *Mtb* growth and reveal potential strategies to mitigate the TB burden among tobacco smokers.

MATERIALS AND METHODS

Study design

Tobacco smoking is associated with pulmonary TB. The goal of the study was to characterize the airspace immune cells of smokers versus nonsmokers at single-cell resolution. BAL samples and matched blood samples were analyzed by scRNA-seq, MILLIPLEX, and flow cytometry. Functional assays of BAL and blood monocytes with *Mtb* were investigated under BSL3 conditions. Samples included in this study were grouped on the basis of smoking status (nonrandomized). Smokers and never smokers were defined according to CDC guidelines as current smokers (everyday smokers; $n = 13$) with ≥100 lifetime cigarettes and never smokers ($n = 21$) who never smoked or smoked fewer than 100 cigarettes in his or her lifetime (table S1 and Supplementary Materials and Methods). Eligible participants underwent bronchoscopy and phlebotomy. Pulmonary function testing was performed for all participants and was within normal limits [interquartile range (IQR) of FEV1 and FVC ≥ 80%]. The performance of different assays was dependent on total BAL cell recovery and cell viability. Experiments and data analysis were performed non-blinded. Experimental replicates varied and are indicated in the figure legend for each panel. The study was approved by the Partners Healthcare Institutional Review Board (IRB; protocol #2013P000063). Participants gave their written informed voluntary consent before inclusion in the study. Detailed inclusion and exclusion criteria and the study protocol are provided in Supplementary Materials and Methods. For functional assays not including BAL sampling, monocytes were isolated from buffy coats of anonymous healthy blood donors collected from the Massachusetts General Hospital Blood Donor Center (Boston, MA) under protocol #2005P001218.

Processing of human samples

BAL fluid was obtained from the right middle lobe and lingula by washing each with 120 ml of saline delivered in 4 × 30 ml aliquots. Samples were combined, filtered through a 70-μm cell strainer, and centrifuged at 4°C for 10 min at 400*g* before resuspending cells in Dulbecco's phosphate-buffered saline (D-PBS; Gibco) and determining cell counts and viability using a NucleoCounter. PBMCs were obtained from whole blood EDTA samples and by density centrifugation using Histopaque (Sigma-Aldrich). Samples were selected on the basis of cell viability (at least 80% or higher) and cell numbers to perform all assays (at least 5×10^6 total cells). Samples for scRNA-seq (nonsmoker $n = 4$; smokers $n = 5$) were selected on the basis of sample availability and viability. All BAL and PBMCs were used freshly for downstream analysis and assays. The BAL fluid was aliquoted and frozen at −80°C until further usage.

Flow cytometry

Cells from BAL or PBMCs were stained with fluorescent-conjugated antibodies and fixable viability dye. For this, cells were washed in

Downloaded from https://www.science.org at Massachusetts Institute of Technology on December 07, 2023

fluorescence-activated cell sorting (FACS) buffer [D-PBS (Gibco) + 1% fetal calf serum (FCS) + 5 mM EDTA (Gibco)] and incubated with 5 μl of Human TruStain FcX receptor blocking solution (BioLegend) for 5 min at room temperature before staining with antibodies for 10 min at room temperature followed by viability staining for 5 min at room temperature. Cells were washed again with magnetic-activated cell sorting (MACS) buffer before fixation in 4% paraformaldehyde. Details for all used antibodies are provided in table S2. Samples were run on an LSRFortessa (BD Biosciences) and analyzed using FlowJo (BD Biosciences).

Cytokine and chemokine detection

BAL fluid was thawed and 30-fold concentrated using Ultra-Centrifugal Filter Units (Millipore). Chemokines and cytokines were measured with a customized MILLIPLEX panel (EMD Millipore) on a Luminex-200 and analyzed using xPONENT 3.1 software (Luminex Corp.). Some of the analyzed data have been analyzed and presented in a previous publication (*12*).

Bulk BAL cells or FACS-sorted airspace monocytes, AMs, and blood monocytes from PBMCs from two smokers (donor 1 and donor 2) were used to determine the inflammatory response of myeloid cells to *Mtb*. A total of 50,000 cells per cell type were plated into a 96-well plate (in duplicates) and either left untreated as a control or exposed to *Mtb* at a multiplicity of infection (MOI) of 1 for 24 hours.

The supernatants from each well were collected, sterile-filtered, and used in a MILLIPLEX assay to measure cytokines and chemokines in each sample using a 5- and 25-plex customized kit (Millipore and R&D Systems). Data were analyzed by calculating the average value of the biological duplicates and then the ratio of *Mtb* treated to control. This was done for each of the measured cytokines. The data were grouped for each sample type (airspace monocyte, AMs, and blood monocytes) and a Kruskal-Wallis with Dunn′s multiple comparisons test to test for significance between airspace monocytes versus AMs and blood monocytes versus AMs.

Monocyte in vitro differentiation

Monocytes were purified from freshly isolated PBMCs by CD14-positive selection using MACS cell separation (Miltenyi Biotec). $CD14^+$ cells were washed with MACS buffer before counting and plated out at 0.1×10^6 $CD14^+$ cells per well in a 96-well plate and RPMI 1640 medium (Gibco) containing 10% human serum. For differentiation into MDMs, cells were incubated for 5 days unless otherwise indicated.

Transwell migration assay

Monocyte in vitro migration toward BAL fluid or recombinant CCL11 (R&D Systems) was determined in a 3-μm Transwell chamber (Corning) by placing PBMCs into the upper well and counting $CD14^+$ viable monocytes in the lower chamber after 3 hours by flow cytometry. Where indicated, PBMCs were pretreated with anti-CCR2 (8 μg/ml; clone 48607, R&D Systems), anti-CCR3 (8 μg/ml; clone 61828, R&D Systems), or anti-CCR5 (5 μg/ml; clone 45531, R&D Systems) blocking antibodies, or BAL fluid was preincubated with an anti-CCL11 (10 μg/ml; clone L403H11, BioLegend), anti-CCL2 (10 μg/ml; clone 2H5, BioLegend), or isotype control antibody (rat IgG1, 10 μg/ml; BioLegend) 30 min before the Transwell assay.

Mtb culture and in vitro infection

Viable *Mtb* H37Rv was used from a freshly thawed stock after the expansion during the exponential growth phase in the 7H9 medium (Middlebrook). The bacteria aliquot was centrifuged at 1200*g* for 5 min and resuspended in phosphate-buffered saline (PBS) before photometric determination of bacterial numbers. The culture was diluted for a MOI of 0.1 in RPMI 1640 + 10% FCS and added to 0.1×10^6 monocytes or macrophages in a 96-well plate. After 2 hours, extracellular bacteria were washed three times with PBS before adding RPMI 1640 + 10% FCS medium. Where indicated, cells were treated with dexamethasone (0.1 μM) or SP600125 (0.1 μM) after uptake of the bacteria and for the remaining time course. At indicated time points, intracellular bacteria were released by incubation of each well with 0.05% Triton X-100 (Sigma-Aldrich) in 200 μl in PBS for 5 min. CFUs were determined by plating out the Triton X-100 treated supernatants on 7H11 agar plates (Middlebrook) in at least two serial dilutions and counting the CFU plates after 3 to 4 weeks of incubation at 37°C in the dark.

scRNA-seq methods

scRNA-seq was conducted using the Seq-Well S^3 protocol (Supplementary Materials and Methods). Briefly, individual cells were loaded in nanowells with poly-dT capture beads. After RNA capture, reverse transcription, second-strand synthesis, and polymerase chain reaction amplification, sequencing libraries were constructed using the Nextera XT DNA Library Preparation Kit. Samples were sequenced on a NovaSeq 6000 and aligned to the Hg19 genome on the Broad Institute′s Terra cloud computing platform. Cells were filtered on the basis of common quality metrics, followed by downstream analyses in Seurat v.4.0.1. RNA velocity analyses were conducted in scVelo and Scanpy, and pseudo-time analyses with Monocle 2. GSEAs were conducted using fgsea (version 1.16.0).

Statistical analysis

All raw, individual-level data for experiments where $n < 20$ are presented in data file S1. All statistical analysis except for scRNA-seq was performed using GraphPad Prism9. For scRNA-seq, Seurat v.4.0.1, scVelo, Scanpy, and Monocle 2 were used for analyses, with Seurat v.4.0.1 and ggplot2 used for plotting. DirichletReg was used to implement Dirichlet regression for scRNA-seq compositional analyses. Data are expressed as median and IQR unless otherwise noted. Each figure legend contains details about the specific statistical test. Data were considered not normally distributed, and analyses were performed using nonparametric tests unless stated otherwise. For datasets comparing two groups, a two-sided nonparametric Wilcoxon test was used. For datasets with more than two groups, a nonparametric one-way or two-way analysis of variance (ANOVA) with post hoc analysis was performed. Differences were considered statistically significant when $P < 0.05$ after correction for multiple hypothesis testing.

Supplementary Materials

This PDF file includes:

Supplementary Materials and Methods
Figs. S1 to S9
Tables S1 to S6

Downloaded from https://www.science.org at Massachusetts Institute of Technology on December 07, 2023

Other Supplementary Material for this manuscript includes the following:
Data file S1
MDAR Reproducibility Checklist

REFERENCES AND NOTES

1. World Health Organization, "Global tuberculosis report 2021" (World Health Organization, 2021).
2. C. R. Horsburgh Jr., C. E. Barry III, C. Lange, Treatment of tuberculosis. *N. Engl. J. Med.* **373**, 2149–2160 (2015).
3. M. Pai, M. A. Behr, D. Dowdy, K. Dheda, M. Divangahi, C. C. Boehme, A. Ginsberg, S. Swaminathan, M. Spigelman, H. Getahun, D. Menzies, M. Raviglione, Tuberculosis. *Nat Rev Dis. Primers* **2**, 16076 (2016).
4. G. A. Amere, P. Nayak, A. D. Salindri, K. M. V. Narayan, M. J. Magee, Contribution of smoking to tuberculosis incidence and mortality in high-tuberculosis-burden countries. *Am. J. Epidemiol.* **187**, 1846–1855 (2018).
5. D. H. Quan, A. J. Kwong, P. M. Hansbro, W. J. Britton, No smoke without fire: The impact of cigarette smoking on the immune control of tuberculosis. *Eur. Respir. Rev.* **31**, 210252 (2022).
6. R. D. Berg, S. Levitte, M. P. O'Sullivan, S. M. O'Leary, C. J. Cambier, J. Cameron, K. K. Takaki, C. B. Moens, D. M. Tobin, J. Keane, L. Ramakrishnan, Lysosomal disorders drive susceptibility to tuberculosis by compromising macrophage migration. *Cell* **165**, 139–152 (2016).
7. L. E. Gleeson, S. M. O'Leary, D. Ryan, A. M. McLaughlin, F. J. Sheedy, J. Keane, Cigarette smoking impairs the bioenergetic immune response to mycobacterium tuberculosis infection. *Am. J. Respir. Cell Mol. Biol.* **59**, 572–579 (2018).
8. S. T. Lugg, A. Scott, D. Parekh, B. Naidu, D. R. Thickett, Cigarette smoke exposure and alveolar macrophages: Mechanisms for lung disease. *Thorax* **77**, 94–101 (2022).
9. S. M. O'Leary, M. M. Coleman, W. M. Chew, C. Morrow, A. M. McLaughlin, L. E. Gleeson, M. P. O'Sullivan, J. Keane, Cigarette smoking impairs human pulmonary immunity to Mycobacterium tuberculosis. *Am. J. Respir. Crit. Care Med.* **190**, 1430–1436 (2014).
10. S. Shang, D. Ordway, M. Henao-Tamayo, X. Bai, R. Oberley-Deegan, C. Shanley, I. M. Orme, S. Case, M. Minor, D. Ackart, L. Hascall-Dove, A. R. Ovrutsky, P. Kandasamy, D. R. Voelker, C. Lambert, B. M. Freed, M. D. Iseman, R. J. Basaraba, E. D. Chan, Cigarette smoke increases susceptibility to tuberculosis—Evidence from in vivo and in vitro models. *J. Infect. Dis.* **203**, 1240–1248 (2011).
11. R. N. van Zyl-Smit, A. Binder, R. Meldau, P. L. Semple, A. Evans, P. Smith, E. D. Bateman, K. Dheda, Cigarette smoke impairs cytokine responses and BCG containment in alveolar macrophages. *Thorax* **69**, 363–370 (2014).
12. B. Corleis, J. L. Cho, S. J. Gates, A. H. Linder, A. Dickey, A. C. Lisanti-Park, A. E. Schiff, M. Ghebremichael, P. Kohli, T. Winkler, R. S. Harris, B. D. Medoff, D. S. Kwon, Smoking and human immunodeficiency virus 1 infection promote retention of $CD8^+$ T cells in the airway Mucosa. *Am. J. Respir. Cell Mol. Biol.* **65**, 513–520 (2021).
13. Y. Hao, S. Hao, E. Andersen-Nissen, W. M. Mauck III, S. Zheng, A. Butler, M. J. Lee, A. J. Wilk, C. Darby, M. Zager, P. Hoffman, M. Stoeckius, E. Papalexi, E. P. Mimitou, J. Jain, A. Srivastava, T. Stuart, L. M. Fleming, B. Yeung, A. J. Rogers, J. M. McElrath, C. A. Blish, R. Gottardo, P. Smibert, R. Satija, Integrated analysis of multimodal single-cell data. *Cell* **184**, 3573–3587. e29 (2021).
14. T. K. Hughes, M. H. Wadsworth II, T. M. Gierahn, T. Do, D. Weiss, P. R. Andrade, F. Ma, B. J. de Andrade Silva, S. Shao, L. C. Tsoi, J. Ordovas-Montanes, J. E. Gudjonsson, R. L. Modlin, J. C. Love, A. K. Shalek, Second-strand synthesis-based massively parallel scRNA-seq reveals cellular states and molecular features of human inflammatory skin pathologies. *Immunity* **53**, 878–894.e7 (2020).
15. C. A. Dutertre, E. Becht, S. E. Irac, A. Khalilnezhad, V. Narang, S. Khalilnezhad, P. Y. Ng, L. L. van den Hoogen, J. Y. Leong, B. Lee, M. Chevrier, X. M. Zhang, P. J. A. Yong, G. Koh, J. Lum, S. W. Howland, E. Mok, J. Chen, A. Larbi, H. K. K. Tan, T. K. H. Lim, P. Karagianni, A. G. Tzioufas, B. Malleret, J. Brody, S. Albani, J. van Roon, T. Radstake, E. W. Newell, F. Ginhoux, Single-cell analysis of human mononuclear phagocytes reveals subset-defining markers and identifies circulating inflammatory dendritic cells. *Immunity* **51**, 573–589.e8 (2019).
16. L. Sikkema, C. Ramírez-Suástegui, D. C. Strobl, T. E. Gillett, L. Zappia, E. Madissoon, N. S. Markov, L.-E. Zaragosi, Y. Ji, M. Ansari, M.-J. Arguel, L. Apperloo, M. Banchero, C. Bécavin, M. Berg, E. Chichelnitskiy, M.-i. Chung, A. Collin, A. C. A. Gay, J. Gote-Schniering, B. Hooshiar Kashani, K. Inecik, M. Jain, T. S. Kapellos, T. M. Kole, S. Leroy, C. H. Mayr, A. J. Oliver, M. von Papen, L. Peter, C. J. Taylor, T. Walzthoeni, C. Xu, L. T. Bui, C. De Donno, L. Dony, A. Faiz, M. Guo, A. J. Gutierrez, L. Heumos, N. Huang, I. L. Ibarra, N. D. Jackson, P. Kadur Lakshminarasimha Murthy, M. Lotfollahi, T. Tabib, C. Talavera-López, K. J. Travaglini, A. Wilbrey-Clark, K. B. Worlock, Lung Biological Network Consortium, An integrated cell atlas of the lung in health and disease. *Nat. Med.* **29**, 1563–1577 (2023).
17. V. Bergen, M. Lange, S. Peidli, F. A. Wolf, F. J. Theis, Generalizing RNA velocity to transient cell states through dynamical modeling. *Nat. Biotechnol.* **38**, 1408–1414 (2020).
18. F. A. Wolf, P. Angerer, F. J. Theis, SCANPY: Large-scale single-cell gene expression data analysis. *Genome Biol.* **19**, 15 (2018).
19. K. Baßler, W. Fujii, T. S. Kapellos, E. Dudkin, N. Reusch, A. Horne, B. Reiz, M. D. Luecken, C. Osei-Sarpong, S. Warnat-Herresthal, L. Bonaguro, J. Schulte-Schrepping, A. Wagner, P. Gunther, C. Pizarro, T. Schreiber, R. Knoll, L. Holsten, C. Kroger, E. De Domenico, M. Becker, K. Handler, C. T. Wohnhaas, F. Baumgartner, M. Kohler, H. Theis, M. Kraut, M. H. Wadsworth 2nd, T. K. Hughes, H. J. Ferreira, E. Hinkley, I. H. Kaltheuner, M. Geyer, C. Thiele, A. K. Shalek, A. Feisst, D. Thomas, H. Dickten, M. Beyer, P. Baum, N. Yosef, A. C. Aschenbrenner, T. Ulas, J. Hasenauer, F. J. Theis, D. Skowasch, J. L. Schultze, Alveolar macrophages in early stage COPD show functional deviations with properties of impaired immune activation. *Front. Immunol.* **13**, 917232 (2022).
20. I. Angelidis, L. M. Simon, I. E. Fernandez, M. Strunz, C. H. Mayr, F. R. Greiffo, G. Tsitsiridis, M. Ansari, E. Graf, T. M. Strom, M. Nagendran, T. Desai, O. Eickelberg, M. Mann, F. J. Theis, H. B. Schiller, An atlas of the aging lung mapped by single cell transcriptomics and deep tissue proteomics. *Nat. Commun.* **10**, 963 (2019).
21. R. D. Chow, M. Majety, S. Chen, The aging transcriptome and cellular landscape of the human lung in relation to SARS-CoV-2. *Nat. Commun.* **12**, 4 (2021).
22. J. D. Morrow, R. P. Chase, M. M. Parker, K. Glass, M. Seo, M. Divo, C. A. Owen, P. Castaldi, D. L. DeMeo, E. K. Silverman, C. P. Hersh, RNA-sequencing across three matched tissues reveals shared and tissue-specific gene expression and pathway signatures of COPD. *Respir. Res.* **20**, 65 (2019).
23. C. X. Yang, H. Shi, I. Ding, S. Milne, A. I. Hernandez Cordero, C. W. T. Yang, E. K. Kim, T. L. Hackett, J. Leung, D. D. Sin, M. Obeidat, Widespread sexual dimorphism in the transcriptome of human airway epithelium in response to smoking. *Sci. Rep.* **9**, 17600 (2019).
24. X. Qiu, Q. Mao, Y. Tang, L. Wang, R. Chawla, H. A. Pliner, C. Trapnell, Reversed graph embedding resolves complex single-cell trajectories. *Nat. Methods* **14**, 979–982 (2017).
25. J. Kantrowitz, A. Sinjab, L. Xu, T. L. M. Dowell, S. Sivakumar, W. Lang, S. Nunomura-Nakamura, J. Fukuoka, G. Nemer, N. Darwiche, H. Chami, A. Tfayli, I. I. Wistuba, P. Scheet, J. Fujimoto, A. E. Spira, H. Kadara, Genome-wide gene expression changes in the normal-appearing airway during the evolution of smoking-associated lung adenocarcinoma. *Cancer Prev. Res.* **11**, 237–248 (2018).
26. A. Kazeros, B. G. Harvey, B. J. Carolan, H. Vanni, A. Krause, R. G. Crystal, Overexpression of apoptotic cell removal receptor MERTK in alveolar macrophages of cigarette smokers. *Am. J. Respir. Cell Mol. Biol.* **39**, 747–757 (2008).
27. M. N. Ballinger, J. W. Christman, Pulmonary macrophages: Overlooked and underappreciated. *Am. J. Respir. Cell Mol. Biol.* **54**, 1–2 (2016).
28. E. Evren, E. Ringqvist, T. Willinger, Origin and ontogeny of lung macrophages: From mice to humans. *Immunology* **160**, 126–138 (2020).
29. T. S. Haugen, B. Nakstad, O. H. Skjonsberg, T. Lyberg, CD14 expression and binding of lipopolysaccharide to alveolar macrophages and monocytes. *Inflammation* **22**, 521–532 (1998).
30. L. Medina-Ruiz, R. Bartolini, G. J. Wilson, D. P. Dyer, F. Vidler, C. E. Hughes, F. Schuette, S. Love, M. Pingen, A. J. Hayes, J. Fu, A. F. Stewart, G. J. Graham, Analysis of combinatorial chemokine receptor expression dynamics using multi-receptor reporter mice. *eLife* **11**, e72418 (2022).
31. C. Shi, E. G. Pamer, Monocyte recruitment during infection and inflammation. *Nat. Rev. Immunol.* **11**, 762–774 (2011).
32. L. R. Antonelli, A. Gigliotti Rothfuchs, R. Goncalves, E. Roffe, A. W. Cheever, A. Bafica, A. M. Salazar, C. G. Feng, A. Sher, Intranasal poly-IC treatment exacerbates tuberculosis in mice through the pulmonary recruitment of a pathogen-permissive monocyte/macrophage population. *J. Clin. Invest.* **120**, 1674–1682 (2010).
33. M. M. Gaidt, T. S. Ebert, D. Chauhan, T. Schmidt, J. L. Schmid-Burgk, F. Rapino, A. A. Robertson, M. A. Cooper, T. Graf, V. Hornung, Human monocytes engage an alternative inflammasome pathway. *Immunity* **44**, 833–846 (2016).
34. C. J. Cambier, K. K. Takaki, R. P. Larson, R. E. Hernandez, D. M. Tobin, K. B. Urdahl, C. L. Cosma, L. Ramakrishnan, Mycobacteria manipulate macrophage recruitment through coordinated use of membrane lipids. *Nature* **505**, 218–222 (2014).
35. H. P. Gideon, T. K. Hughes, C. N. Tzouanas, M. H. Wadsworth II, A. A. Tu, T. M. Gierahn, J. M. Peters, F. F. Hopkins, J. R. Wei, C. Kummerlowe, N. L. Grant, K. Nargan, J. Y. Phuah, H. J. Borish, P. Maiello, A. G. White, C. G. Winchell, S. K. Nyquist, S. K. C. Ganchua, A. Myers, K. V. Patel, C. L. Ameel, C. T. Cochran, S. Ibrahim, J. A. Tomko, L. J. Frye, J. M. Rosenberg, A. Shih, M. Chao, E. Klein, C. A. Scanga, J. Ordovas-Montanes, B. Berger, J. T. Mattila, R. Madansein, J. C. Love, P. L. Lin, A. Leslie, S. M. Behar, B. Bryson, J. L. Flynn, S. M. Fortune, A. K. Shalek, Multimodal profiling of lung granulomas in macaques reveals cellular correlates of tuberculosis control. *Immunity* **55**, 827–846 (2022).
36. S. B. Cohen, B. H. Gern, J. L. Delahaye, K. N. Adams, C. R. Plumlee, J. K. Winkler, D. R. Sherman, M. Y. Gerner, K. B. Urdahl, Alveolar macrophages provide an early mycobacterium tuberculosis niche and initiate dissemination. *Cell Host Microbe* **24**, 439–446.e4 (2018).

Downloaded from https://www.science.org at Massachusetts Institute of Technology on December 07, 2023

37. L. Huang, E. V. Nazarova, S. Tan, Y. Liu, D. G. Russell, Growth of Mycobacterium tuberculosis in vivo segregates with host macrophage metabolism and ontogeny. *J. Exp. Med.* **215**, 1135–1152 (2018).
38. L. E. Mendonca, E. Pernet, N. Khan, J. Sanz, E. Kaufmann, J. Downey, A. Grant, M. Orlova, E. Schurr, C. Krawczyk, R. G. Jones, L. B. Barreiro, M. Divangahi, Human alveolar macrophage metabolism is compromised during *Mycobacterium tuberculosis* infection. *Front. Immunol.* **13**, 1044592 (2023).
39. S. G. S. Verberk, K. E. de Goede, F. S. Gorki, X. van Dierendonck, R. J. Arguello, J. Van den Bossche, An integrated toolbox to profile macrophage immunometabolism. *Cell Rep. Methods* **2**, 100192 (2022).
40. R. Karimi, G. Tornling, J. Grunewald, A. Eklund, C. M. Sköld, Cell recovery in bronchoalveolar lavage fluid in smokers is dependent on cumulative smoking history. *PLOS ONE* **7**, e34232 (2012).
41. J. M. Löfdahl, J. Wahlström, C. M. Sköld, Different inflammatory cell pattern and macrophage phenotype in chronic obstructive pulmonary disease patients, smokers and non-smokers. *Clin. Exp. Immunol.* **145**, 428–437 (2006).
42. W. A. Wallace, M. Gillooly, D. Lamb, Intra-alveolar macrophage numbers in current smokers and non-smokers: A morphometric study of tissue sections. *Thorax* **47**, 437–440 (1992).
43. V. Chilunda, P. Martinez-Aguado, L. C. Xia, L. Cheney, A. Murphy, V. Veksler, V. Ruiz, T. M. Calderon, J. W. Berman, Transcriptional changes in CD16$^+$ monocytes may contribute to the pathogenesis of COVID-19. *Front. Immunol.* **12**, 665773 (2021).
44. E. Stephenson, G. Reynolds, R. A. Botting, F. J. Calero-Nieto, M. D. Morgan, Z. K. Tuong, K. Bach, W. Sungnak, K. B. Worlock, M. Yoshida, N. Kumasaka, K. Kania, J. Engelbert, B. Olabi, J. S. Spegarova, N. K. Wilson, N. Mende, L. Jardine, L. C. S. Gardner, I. Goh, D. Horsfall, J. McGrath, S. Webb, M. W. Mather, R. G. H. Lindeboom, E. Dann, N. Huang, K. Polanski, E. Prigmore, F. Gothe, J. Scott, R. P. Payne, K. F. Baker, A. T. Hanrath, I. C. D. S. van der Loeff, A. S. Barr, A. Sanchez-Gonzalez, L. Bergamaschi, F. Mescia, J. L. Barnes, E. Kilich, A. de Wilton, A. Saigal, A. Saleh, S. M. Janes, C. M. Smith, N. Gopee, C. Wilson, P. Coupland, J. M. Coxhead, V. Y. Kiselev, S. van Dongen, J. Bacardit, H. W. King, Cambridge Institute of Therapeutic Immunology and Infectious Disease-National Institute of Health Research (CITIID-NIHR) COVID-19 BioResource Collaboration, A. J. Rostron, A. J. Simpson, S. Hambleton, E. Laurenti, P. A. Lyons, K. B. Meyer, M. Z. Nikolic, C. J. A. Duncan, K. G. C. Smith, S. A. Teichmann, M. R. Clatworthy, J. C. Marioni, B. Gottgens, M. Haniffa, Single-cell multi-omics analysis of the immune response in COVID-19. *Nat Med* **27**, 904–916 (2021).
45. D. Wendisch, O. Dietrich, T. Mari, S. von Stillfried, I. L. Ibarra, M. Mittermaier, C. Mache, R. L. Chua, R. Knoll, S. Timm, S. Brumhard, T. Krammer, H. Zauber, A. L. Hiller, A. Pascual-Reguant, R. Mothes, R. D. Bulow, J. Schulze, A. M. Leipold, S. Djudjaj, F. Erhard, R. Geffers, F. Pott, J. Kazmierski, J. Radke, P. Pergantis, K. Bassler, C. Conrad, A. C. Aschenbrenner, B. Sawitzki, M. Landthaler, E. Wyler, D. Horst, C.-O. I. Deutsche, S. Hippenstiel, A. Hocke, F. L. Heppner, A. Uhrig, C. Garcia, F. Machleidt, S. Herold, S. Elezkurtaj, C. Thibeault, M. Witzenrath, C. Cochain, N. Suttorp, C. Drosten, C. Goffinet, F. Kurth, J. L. Schultze, H. Radbruch, M. Ochs, R. Eils, H. Muller-Redetzky, A. E. Hauser, M. D. Luecken, F. J. Theis, C. Conrad, T. Wolff, P. Boor, M. Selbach, A. E. Saliba, L. E. Sander, SARS-CoV-2 infection triggers profibrotic macrophage responses and lung fibrosis. *Cell* **184**, 6243–6261.e27 (2021).
46. K. A. Khan, J. L. McMurray, F. Mohammed, R. Bicknell, C-type lectin domain group 14 proteins in vascular biology, cancer and inflammation. *FEBS J.* **286**, 3299–3332 (2019).
47. E. P. McGreal, N. Ikewaki, H. Akatsu, B. P. Morgan, P. Gasque, Human C1qRp is identical with CD93 and the mNI-11 antigen but does not bind C1q. *J. Immunol.* **168**, 5222–5232 (2002).
48. D. M. Conroy, T. J. Williams, Eotaxin and the attraction of eosinophils to the asthmatic lung. *Respir. Res.* **2**, 150–156 (2001).
49. R. Martinelli, I. Sabroe, G. LaRosa, T. J. Williams, J. E. Pease, The CC chemokine eotaxin (CCL11) is a partial agonist of CC chemokine receptor 2b. *J. Biol. Chem.* **276**, 42957–42964 (2001).
50. L. Fantuzzi, P. Borghi, V. Ciolli, G. Pavlakis, F. Belardelli, S. Gessani, Loss of CCR2 expression and functional response to monocyte chemotactic protein (MCP-1) during the differentiation of human monocytes: Role of secreted MCP-1 in the regulation of the chemotactic response. *Blood* **94**, 875–883 (1999).
51. A. Menzies-Gow, S. Ying, I. Sabroe, V. L. Stubbs, D. Soler, T. J. Williams, A. B. Kay, Eotaxin (CCL11) and eotaxin-2 (CCL24) induce recruitment of eosinophils, basophils, neutrophils, and macrophages as well as features of early- and late-phase allergic reactions following cutaneous injection in human atopic and nonatopic volunteers. *J. Immunol.* **169**, 2712–2718 (2002).
52. A. W. Mould, K. I. Matthaei, I. G. Young, P. S. Foster, Relationship between interleukin-5 and eotaxin in regulating blood and tissue eosinophilia in mice. *J. Clin. Invest.* **99**, 1064–1071 (1997).
53. B. B. Mishra, V. A. Rathinam, G. W. Martens, A. J. Martinot, H. Kornfeld, K. A. Fitzgerald, C. M. Sassetti, Nitric oxide controls the immunopathology of tuberculosis by inhibiting NLRP3 inflammasome-dependent processing of IL-1β. *Nat. Immunol.* **14**, 52–60 (2013).
54. D. M. Tobin, Host-directed therapies for tuberculosis. *Cold Spring Harb. Perspect. Med.* **5**, a021196 (2015).
55. C. J. Cambier, S. M. O'Leary, M. P. O'Sullivan, J. Keane, L. Ramakrishnan, Phenolic glycolipid facilitates mycobacterial escape from microbicidal tissue-resident macrophages. *Immunity* **47**, 552–565.e4 (2017).
56. L. Lavalett, H. Ortega, L. F. Barrera, Infection of monocytes from tuberculosis patients with two virulent clinical isolates of *Mycobacterium Tuberculosis* induces alterations in myeloid effector functions. *Front. Cell. Infect. Microbiol.* **10**, 163 (2020).
57. A. Novikov, M. Cardone, R. Thompson, K. Shenderov, K. D. Kirschman, K. D. Mayer-Barber, T. G. Myers, R. L. Rabin, G. Trinchieri, A. Sher, C. G. Feng, Mycobacterium tuberculosis triggers host type I IFN signaling to regulate IL-1β production in human macrophages. *J. Immunol.* **187**, 2540–2547 (2011).
58. G. S. Olson, T. A. Murray, A. N. Jahn, D. Mai, A. H. Diercks, E. S. Gold, A. Aderem, Type I interferon decreases macrophage energy metabolism during mycobacterial infection. *Cell Rep.* **35**, 109195 (2021).
59. G. Meintjes, C. Stek, L. Blumenthal, F. Thienemann, C. Schutz, J. Buyze, R. Ravinetto, H. van Loen, A. Nair, A. Jackson, R. Colebunders, G. Maartens, R. J. Wilkinson, L. Lynen, PredART Trial Team, Prednisone for the prevention of paradoxical tuberculosis-associated iris. *N. Engl. J. Med.* **379**, 1915–1925 (2018).
60. C. Schutz, A. G. Davis, B. Sossen, R. P. Lai, M. Ntsekhe, Y. X. Harley, R. J. Wilkinson, Corticosteroids as an adjunct to tuberculosis therapy. *Expert Rev. Respir. Med.* **12**, 881–891 (2018).
61. A. V. Misharin, L. Morales-Nebreda, P. A. Reyfman, C. M. Cuda, J. M. Walter, A. C. McQuattie-Pimentel, C. I. Chen, K. R. Anekalla, N. Joshi, K. J. N. Williams, H. Abdala-Valencia, T. J. Yacoub, M. Chi, S. Chiu, F. J. Gonzalez-Gonzalez, K. Gates, A. P. Lam, T. T. Nicholson, P. J. Homan, S. Soberanes, S. Dominguez, V. K. Morgan, R. Saber, A. Shaffer, M. Hinchcliff, S. A. Marshall, A. Bharat, S. Berdnikovs, S. M. Bhorade, E. T. Bartom, R. I. Morimoto, W. E. Balch, J. I. Sznajder, N. S. Chandel, G. M. Mutlu, M. Jain, C. J. Gottardi, B. D. Singer, K. M. Ridge, N. Bagheri, A. Shilatifard, G. R. S. Budinger, H. Perlman, Monocyte-derived alveolar macrophages drive lung fibrosis and persist in the lung over the life span. *J. Exp. Med.* **214**, 2387–2404 (2017).
62. C. E. Barry III, H. I. Boshoff, V. Dartois, T. Dick, S. Ehrt, J. Flynn, D. Schnappinger, R. J. Wilkinson, D. Young, The spectrum of latent tuberculosis: Rethinking the biology and intervention strategies. *Nat. Rev. Microbiol.* **7**, 845–855 (2009).
63. M. T. Coleman, P. Maiello, J. Tomko, L. J. Frye, D. Fillmore, C. Janssen, E. Klein, P. L. Lin, Early changes by ^{18}fluorodeoxyglucose positron emission tomography coregistered with computed tomography predict outcome after Mycobacterium tuberculosis infection in cynomolgus macaques. *Infect. Immun.* **82**, 2400–2404 (2014).
64. Y. Shao, H. Song, G. Li, Y. Li, Y. Li, L. Zhu, W. Lu, C. Chen, Relapse or re-infection, the situation of recurrent tuberculosis in eastern China. *Front. Cell. Infect. Microbiol.* **11**, 638990 (2021).
65. A. van Rie, R. Warren, M. Richardson, T. C. Victor, R. P. Gie, D. A. Enarson, N. Beyers, P. D. van Helden, Exogenous reinfection as a cause of recurrent tuberculosis after curative treatment. *N. Engl. J. Med.* **341**, 1174–1179 (1999).
66. S. Verver, R. M. Warren, N. Beyers, M. Richardson, G. D. van der Spuy, M. W. Borgdorff, D. A. Enarson, M. A. Behr, P. D. van Helden, Rate of reinfection tuberculosis after successful treatment is higher than rate of new tuberculosis. *Am. J. Respir. Crit. Care Med.* **171**, 1430–1435 (2005).
67. R. J. Blount, H. Phan, T. Trinh, H. Dang, C. Merrifield, M. Zavala, J. Zabner, A. P. Comellas, E. M. Stapleton, M. R. Segal, J. Balmes, N. V. Nhung, P. Nahid, Indoor air pollution and susceptibility to tuberculosis infection in urban Vietnamese children. *Am. J. Respir. Crit. Care Med.* **204**, 1211–1221 (2021).
68. N. Jafta, P. M. Jeena, L. Barregard, R. N. Naidoo, Association of childhood pulmonary tuberculosis with exposure to indoor air pollution: A case control study. *BMC Public Health* **19**, 275 (2019).

Acknowledgments: We would like to acknowledge the contributions of the Ragon Institute Imaging Core Facility and the BSL3 facility. We also thank the staff from the Massachusetts General Hospital. We would also like to thank F. Ruzicka, S. Ip, D. Worrall, M. Kone, V. Kelly, and the Pulmonary Special Procedures Unit for assistance with this study. *Mtb* H37Rv was provided by S. Fortune, Harvard T. H. Chan School of Public Health. A fluorescent strain of *Mtb* H37Rv (mCherry) was provided by S. H. E. Kaufmann, Max Planck Institute of Infection Biology, Berlin. **Funding:** This work was supported by NIH grant NIH 1U01HL121827-01 (to B.D.M. and D.S.K.), NIH grant NIH 1R01DA042685-01 (to D.S.K.), NIH grant NIH 5U24AI118672 (to A.K.S.), NIH grant NIH DP2OD020839 (to A.K.S.), Ragon Institute of MGH, MIT, and Harvard (to A.K.S.), Beckman Young Investigator Award (to A.K.S.), Alfred P. Sloan Research Fellowship in Chemistry (to A.K.S.), National Science Foundation Graduate Research Fellowship (1122374, to C.N.T.), Fannie and John Hertz Foundation Fellowship (to C.N.T.), and German Research Foundation individual research grant "TB compare" CO 224/2-1 (to B.C.). **Author contributions:** B.C., J.L.C., B.D.M., A.K.S., and D.S.K. conceptualized the study. B.C., C.N.T., M.H.W., J.L.C., A.D., B.D.M., A.K.S., and D.S.K. developed the methodology. B.C., C.N.T., M.H.W., J.L.C., A.H.L., A.E.S., A.K.D., F.S., and B.Z. performed experiments and analyzed the data (investigation). B.C., C.N.T., and M.H.W. visualized the data. B.C., B.D.M., A.K.S., and D.S.K. provided supervision. B.C. and C.N.T. wrote the original draft. B.C., C.N.T., M.H.W., J.L.C., B.D.M., A.K.S., D.S.K., F.S., B.Z., and A.D. reviewed and edited the

Downloaded from https://www.science.org at Massachusetts Institute of Technology on December 07, 2023

manuscript. **Competing interests:** A.K.S. reports compensation for consulting or scientific advisory board (SAB) membership from Merck, Honeycomb Biotechnologies, Cellarity, Repertoire Immune Medicines, Hovione, Third Rock Ventures, Ochre Bio, FL82, FL86, Empress Therapeutics, Relation Therapeutics, Senda Biosciences, IntrECate Biotherapeutics, Santa Ana Bio, Janssen, and Dahlia Biosciences unrelated to this work. B.D.M. reports compensation for consulting work from Sanofi and Regeneron. B.D.M. has also received research funding from Bayer, Sanofi, Boehringer Ingelheim, and Regeneron. D.S.K. is a scientific cofounder and a consultant for Day Zero Diagnostics unrelated to this work. **Data and materials availability:** All data associated with this study are present in the paper or the Supplementary Materials. Materials generated during the current study are available from the corresponding authors under an MTA with the Ragon Institute of MGH, MIT, and Harvard. All codes used for scRNA-seq analysis are accessible at Zenodo under https://zenodo.org/records/10020227. scRNA-seq digital gene expression matrices, metadata, and interactive visualization tools can be found in studies SCP2409 (bronchoalveolar lavage samples; https://singlecell.broadinstitute.org/single_cell/study/SCP2409) and SCP2410 (peripheral blood samples; https://singlecell.broadinstitute.org/single_cell/study/SCP2410) through the Alexandria Project, a Bill & Melinda Gates Foundation–funded portal (part of the Single Cell Portal hosted by the Broad Institute of MIT and Harvard). FASTQ data for scRNA-seq are available upon request and with a data use agreement. Datasets from reanalyzed studies are available at https://cellxgene.cziscience.com/collections/6f6d381a-7701-4781-935c-db10d30de293 (Human Lung Cell Atlas) and https://singlecell.broadinstitute.org/single_cell/study/SCP1749/cellular-ecology-of-m-tuberculosis-granulomas-4-week-dataset (Gideon *et al.*).

Submitted 17 December 2022
Accepted 7 November 2023
Published 6 December 2023
10.1126/scitranslmed.adg3451

Downloaded from https://www.science.org at Massachusetts Institute of Technology on December 07, 2023

Science Translational Medicine

Tobacco smoke exposure recruits inflammatory airspace monocytes that establish permissive lung niches for *Mycobacterium tuberculosis*

Björn Corleis, Constantine N. Tzouanas, Marc H. Wadsworth, II, Josalyn L. Cho, Alice H. Linder, Abigail E. Schiff, Björn Zessin, Fabian Stei, Anca Dorhoi, Amy K. Dickey, Benjamin D. Medoff, Alex K. Shalek, and Douglas S. Kwon

Sci. Transl. Med. **15** (725), eadg3451. DOI: 10.1126/scitranslmed.adg3451

View the article online
https://www.science.org/doi/10.1126/scitranslmed.adg3451
Permissions
https://www.science.org/help/reprints-and-permissions

Downloaded from https://www.science.org at Massachusetts Institute of Technology on December 07, 2023

Use of this article is subject to the Terms of service

Science Translational Medicine (ISSN 1946-6242) is published by the American Association for the Advancement of Science. 1200 New York Avenue NW, Washington, DC 20005. The title *Science Translational Medicine* is a registered trademark of AAAS.

Copyright © 2023 The Authors, some rights reserved; exclusive licensee American Association for the Advancement of Science. No claim to original U.S. Government Works